INL/EXT-16-39582

# Small Sample Reactivity Measurements in the RRR/SEG Facility: Reanalysis using TRIPOLI-4

Andrew Hummel
Giuseppe Palmiotti

August 2016

Idaho National Laboratory

The INL is a U.S. Department of Energy National Laboratory
operated by Battelle Energy Alliance

INL/EXT-16-39582

# Small Sample Reactivity Measurements in the RRR/SEG Facility: Reanalysis using TRIPOLI-4

Andrew Hummel
Giuseppe Palmiotti

August 2016

Idaho National Laboratory
Idaho Falls, Idaho 83415

http://www.inl.gov

Prepared for the
U.S. Department of Energy
Assistant Secretary for ____, OR Office of _____
Under DOE Idaho Operations Office
Contract DE-AC07-05ID14517

# SUMMARY

This work involved reanalyzing the RRR/SEG integral experiments performed at the Rossendorf facility in Germany throughout the 1970s and 80s. These small sample reactivity worth measurements were carried out using the pile oscillator technique for many different fission products, structural materials, and standards. The coupled fast-thermal system was designed such that the measurements would provide insight into elemental data, specifically the competing effects between neutron capture and scatter. Comparing the measured to calculated reactivity values can then provide adjustment criteria to ultimately improve nuclear data for fast reactor designs. Due to the extremely small reactivity effects measured (typically less than 1 pcm) and the specific heterogeneity of the core, the tool chosen for this analysis was TRIPOLI-4. This code allows for high fidelity 3-dimensional geometric modeling, and the most recent, unreleased version, is capable of exact perturbation theory. Within the framework of the CEA-DOE agreement, Andrew Hummel spent three months at the CEA Cadarache utilizing this newest version of TRIPOLI.

# ACKNOWLEDGEMENTS

This work was carried out in conjunction with the Department of Energy, the Idaho National Laboratory, and the Commissariat for Atomic Energy and Alternative Energies (CEA) at Cadarache. The author is incredibly grateful to the host research center, particularly Cyrille de Saint Jean, Gerald Rimpault, and Pierre Leconte for their mentoring, patience, and extraordinary hospitality.

## CONTENTS

## FIGURES

## TABLES

# ACRONYMS

| | |
|---|---|
| C/E | Nomenclature signifying the Calculated divided by the Experimental value |
| CE | Continuous Energy |
| CRW | Central Reactivity Worth |
| EPT | Exact Perturbation Theory |
| IFP | Iterated Fission Probability |
| MC | Monte Carlo |
| MCNP | Monte Carlo Neutral Particle |
| PCM | Percent milli-rho |
| PUWO | Probe-Untergrund-Wechseloszillator |
| RRR | Rossendorf Research Reactor |
| SEG | Schnelles Einsatz-Gitter |

# 1. INTRODUCTION

The Rossendorf Research Reactor (RRR), or Rossendorfer Ringzonenreacktor, was a zero power research reactor located at the Rossendorf research facility in Germany just east of Dresden. It first reached criticality on December 16, 1962 [1] and has recently been decommissioned with all the fuel removed in 2000[a] [2]. The RRR was based off the Argonaut reactor design which consisted of an annular core surrounded by a graphite reflector. It also contained a removable internal graphite reflector. This internal reflector was replaced in December of 1972 with a rapid deployment lattice known as Schnelles Einsatz-Gitter (SEG) [3]. The insertion of the SEG experimental lattice leads to a fast-thermal coupled system with the annular RRR reactor acting as the thermal driver to the fast SEG lattice. A converter material is placed between these two zones to increase the importance of high energy neutrons and better allow the fast spectrum to reach equilibrium. The RRR/SEG integral experimental setup was used to perform small sample reactivity measurements for fission product nuclides, common structural materials, and standards[4]. The samples were placed in the central channel of the SEG lattice and the pile oscillator method was used to measure the reactivity.

The significance of these measurements results from the ability to manipulate the adjoint spectrum by using different material in the SEG fuel. Because the general shape of the adjoint function in a fast system has a depression around 10 keV with sharp increases at lower and higher energies, the different SEG lattices were designed to have either a very strongly energy dependent or independent adjoint function. If the adjoint is flat or energy-independent, the reactivity change can be attributed to the absorption component of the sample material. If the adjoint is steep or monotonically rising, the reactivity change is dominated by the scattering component of the sample material.

A total of 10 integral experimental setups (SEG lattice configurations) were constructed. This evaluation focuses on the reactivity measurements taken between 1988 and 1990 on the SEG 4, 5, 6 EK-10, 6 EK-45, 7A, and 7B configurations[b] as these were arranged in clean geometry (sample, container, experimental channel filling). This was achieved by filling the oscillating tube with graphite bars and inserting the samples into graphite containers that would then oscillate against an equivalent graphite dummy element[c] [4].

Many publications, reports, and conference proceedings have analyzed the SEG results in both English [5-19] and German [20, 21] in order to better quantify neutron cross section data. However, this work is the first to use continuous energy Monte Carlo. MCNP6.1 [22] was initially employed with the intent on using eigenvalue differencing, but this simplistic approach proved ill suitable due to the extremely small reactivity effects measured [23]. Thus the French code TRIPOLI-4 [24] was chosen for its capability of performing exact perturbation theory. Although this capability is not available in the most recently released version of this code, special access was granted for this work. All results and discussions are related to this unreleased version of TRIPOLI-4 unless otherwise stated.

---

[a] References 1 and 3 were originally written in German and the information comes from a translated version.

[b] Although Klaus Dietze[4] has extensively compiled the experimental measurements and reports, missing information has limited the extent to which some of these configurations have been analyzed.

[c] The measurements on SEG4 were originally performed under the same conditions as SEG 1-3 in which the oscillating tube was voided.

## 1.1 Spectral Characteristics

It is well known that the energy dependence of the adjoint flux in fast systems is characterized by a depression around 10 keV with rapid increases to higher and lower energies due to the higher fission neutron yield per absorption at these energies [25]. The SEG lattices were thus filled with specific arrangements of pellets such that the adjoint flux would exhibit either a flat or very steep dependence on energy. This energy dependence allows one to observe the competing effects due to capture and scatter independently and thus formulate uncertainty information on each of these elemental phenomena. To confirm the shape of the adjoint, also referred to as the importance function, the pile oscillator method was used to activate the following photoneutron sources: RaBe (energy ~ 3 MeV), NaBe (energy ~ 1 MeV), NaD (energy ~ 300 keV), and SbBe (energy ~ 24 keV) sources [3]. Equation (1) shows the relationship between the importance function, $\phi^{\dagger}$, and the pseudo-reactivity worths, $\rho^*$, of these different neutron sources measured in the central channel.

$$\rho^*(P,r) = \frac{Q}{F(R)} \int q(E)\phi^{\dagger}(E,r)dE \tag{1}$$

Relating these to the central reactivity worth of the standard $B_4C$, and dividing by the source strength, $Q$, the pseudo-reactivity becomes proportional to the importance function in the given energy range of the neutron spectrum, $q$, emitted [6], [26].

$$\frac{\rho_j^*}{Q_i} \sim \sum_i q_{ij}\phi_i^{\dagger} \tag{2}$$

Further verification of the adjoint shape was determined by examining the reactivity effect due to pure scattering materials such as H, D, and C. The forward flux was typically measured with a boron ionization chamber, but proton recoil spectroscopy, Li-6 sandwich spectroscopy, stilbene scintillation, and foil activation were also used [27].

The SEG 4, 5, 7A, and 7B configurations are characterized by having an energy-independent or flat importance function, signifying that all reactivity effects can be attributed solely to capture. At high energies this is accomplished by minimizing the concentration of those isotopes that have large propensities for fast fission. This is achieved by reducing the U-238 content in the system as much as possible. The importance function can be decreased or flattened at lower energies by introducing a strong neutron poison (i.e. $1/\nu$ absorber material) into the system. Cadmium was used in the SEG 4 pellet cell, but due to the observed Cd discrepancy found in the self-shielding treatment in the resonance region, borated graphite was used in SEG 5 and 7 [12]. Additionally, the scattering material polyethylene was introduced in SEG 7A and 7B to soften the neutron spectrum.

To contrast this flat behavior, a newly designed SEG 6 lattice (shown in Figures 1.1 and 1.2) was built to have a very strongly energy-dependent or steep adjoint flux. This ultimately enhances the effect due to scattering and can be achieved in one of two ways: if $d\Psi^+/dE < 0$, the reactivity effect will be positive, and if $d\Psi^+/dE > 0$, the effect will be negative. The former can only be achieved with near pure fissile material. Since all the fuel came from Russia and was limited to 36%, the latter possibility was the only option. Therefore, each moderation or down scatter event will decrease the importance function. To achieve this behavior a strong $1/\nu$ neutron absorbing material (borated carbon) was introduced near the sample to minimize the thermal contribution.

Additionally, the fast contribution is maximized by increasing the U-238 content in the system as much as possible. Compounding this is the fact that the absorption cross-section decreases at higher energies (harder spectra) for most all structural materials, making the SEG 6 integral experiments especially well-suited for examining inelastic cross-section data.

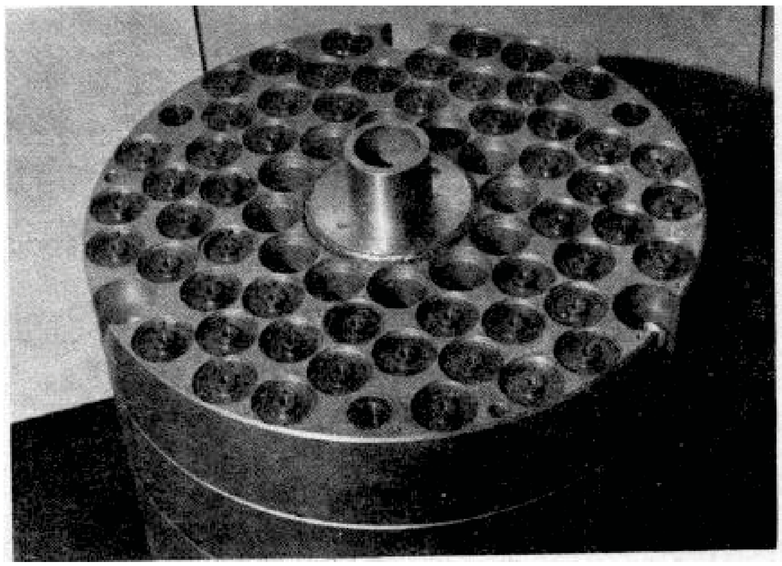

Figure 1.1. SEG6 lattice with EK_45 inner absorption zone inserted [9].

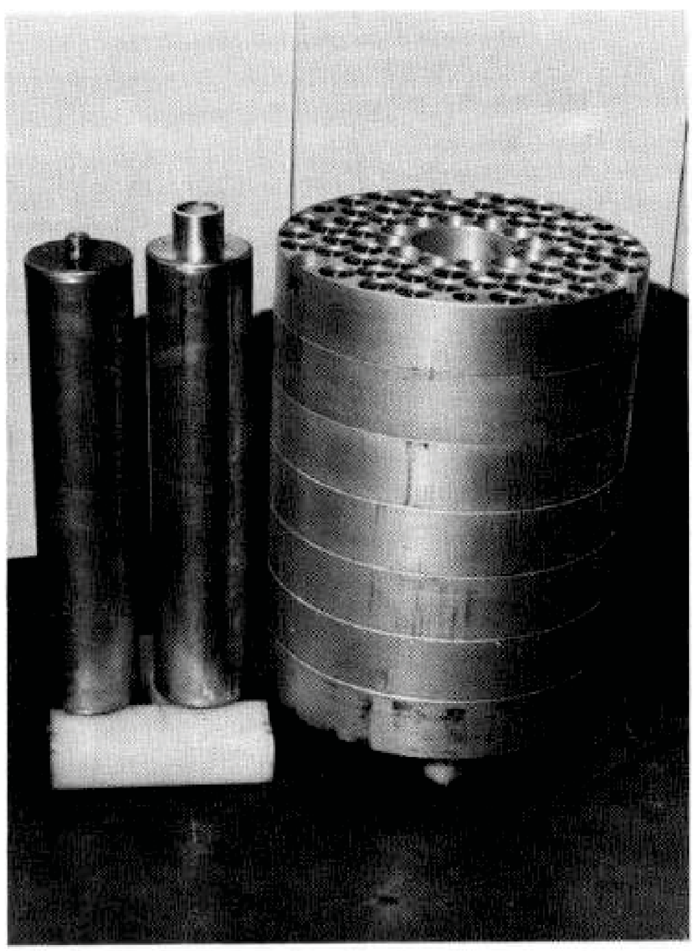

Figure 1.2. SEG6 lattice with both EK_10 and EK_45 inner absorption zones [13].

## 1.2 OSCILLATION MEASUREMENTS

The RRR/SEG integral experimental setup was used for nearly two decades to perform small sample reactivity measurements using the pile oscillator technique. The samples consisted of thin wires or small disks, as seen in Figures 1.3 and 1.4, that were placed in graphite containers and inserted in the central channel via an experimental aluminum oscillating tube. The oscillating tube was filled with graphite bars and the samples oscillated against an equivalent dummy graphite container. The central zone and oscillating tube for the SEG 6 arrangements, however, were filled with boron carbide powder.

The pile oscillator method involves modulation of the neutron flux from an oscillating sample between regions of high and low neutron flux [28]. Described by Foell: "*Reactivity and the total neutron population undergo oscillations with the same frequency as the oscillations of the sample. The neutron population oscillation gives rise to a corresponding signal in a neutron-sensitive detector located in or near the reactor. Because the amplitude of the oscillation is related to neutron interaction with the sample, information about the cross sections of the sample may be inferred by comparing the results with those obtained from samples with known cross sections* (p.42)." This process was first proposed by E. Wigner during the Manhattan Project and later described by Weinberg and Schweinler [29].

The pneumatically driven oscillator was inserted in the SEG lattice in a square-wave manner with a 20.48 second period and 80 cm stroke [4]. A boron ionization chamber with a 256 channel memory detected the flux response which was used to generate the reactivity vs. time behavior using the inverse point kinetics equations. As Dietze claims, "*The sample reactivity is identical with the reactivity difference in the two oscillator positions* (p.13)."

This method is highly accurate and depends on the reactor power level, the number of measured periods, and how exactly positioned (and reproducible) the oscillator tube and its inner parts are. For these measurements, a special oscillator (seen in Figures 1.5 and 1.6) known as Probe-Untergrund-Wechseloszillator (PUWO) was used to guarantee constancy. The reactivity effect and background were measured simultaneously without removing the oscillator tube by having a periodic and automatic insertion of a sample replacement container (minus the sample itself) [6]. With the reactor power constant at approximately 50 watts and a measuring time of 12 hours, reactivity effects were measured to an accuracy of roughly +/- 0.3 millicents. The inherent accuracy associated with the reactor drift behavior and neutron chain reaction (i.e. the statistical fluctuation in the number of neutrons produced in a given fission event) was found to be about +/- 0.1 millicents. After 1000 cycles an accuracy down to $\Delta k/k < 10^{-8}$ could be achieved. The micro-processor system MPS 4944 was used to control the measurement, store the flux response, and perform the on-line reactivity calculation.

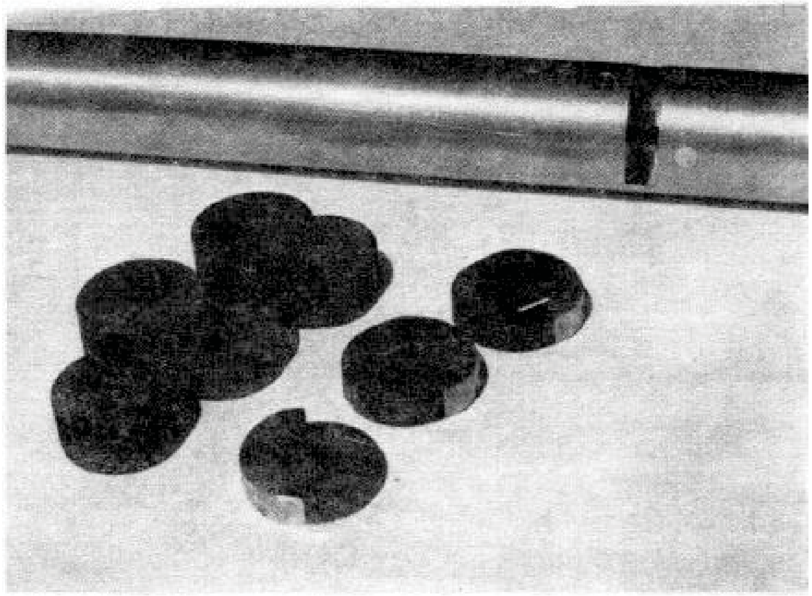
Figure 1.3. Small sample disks and aluminum oscillator tube [9].

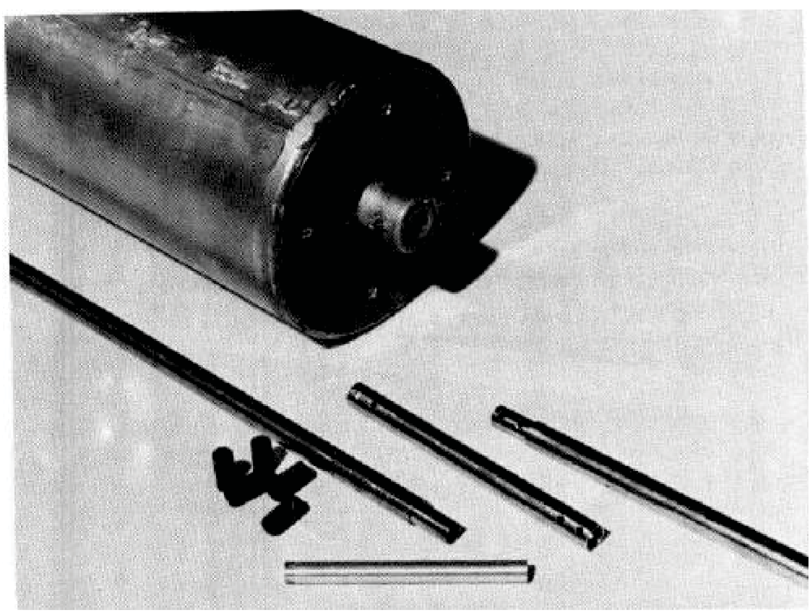
Figure 1.4. Thin wire samples and EK_10 absorption zone [9].

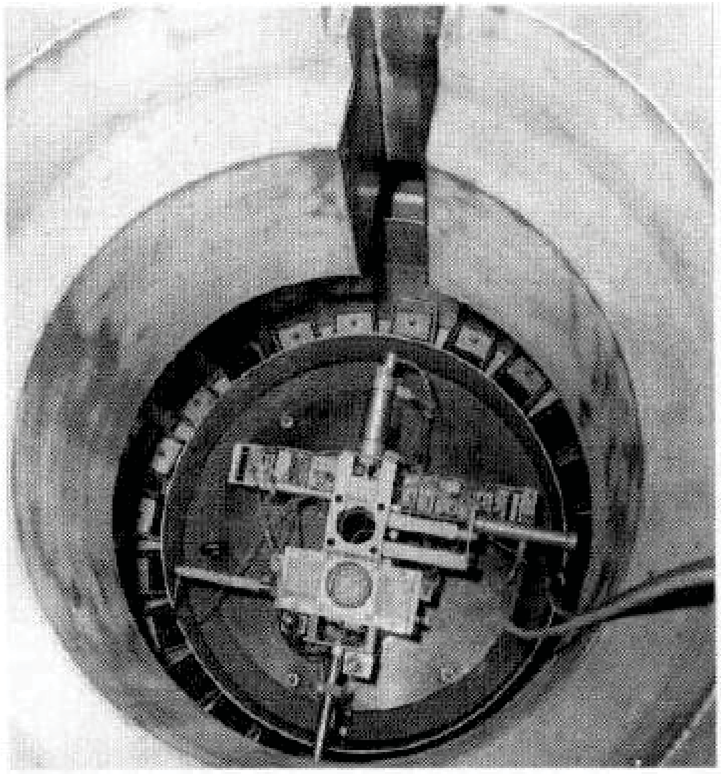

Figure 1.5. PUWO oscillator on top of RRR/SEG [6].

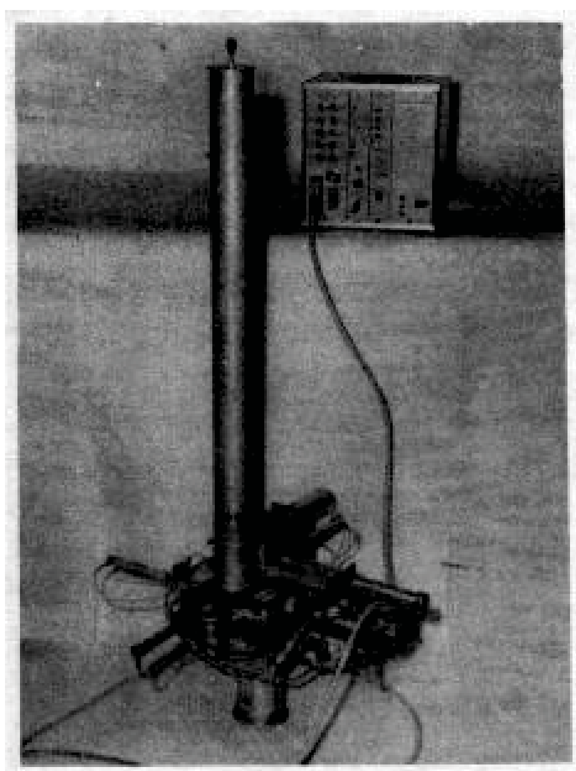

Figure 1.6. PUWO oscillator [9].

# 2. METHODOLOGY

The oscillation of samples will induce small reactivity changes or perturbations in the reactor system. Using diffusion theory, the reactivity change can be separated according to the individual reactions that take place in the sample as shown in Equation (3) [30].

$$\rho = \rho_a + \rho_s + \rho_f + \rho_d \tag{3}$$

These four components represent absorption, scatter, fission, and diffusion. If these perturbations are small enough (i.e. if they don't trigger feedback effects) then these terms can be expressed in terms of unperturbed fluxes as given in Equations (4) – (7) [31].

$$\rho_a = \frac{1}{F}\left\{-\int_V \int_E dV\, dE\phi\,(r,E)\phi^{\dagger}(r,E)\right\} \tag{4}$$

$$\rho_s = \frac{1}{F}\left\{\int_V \int_E \int_{E'} dVdEdE'\phi(r,E)\Delta\Sigma_s(r,E,E')[\phi^{\dagger}(r,E') - \phi^{\dagger}(r,E)]\right\} \tag{5}$$

$$\rho_f = \frac{1}{F}\left\{\int_V \int_E \int_{E'} dVdEdE'\phi(r,E)\nu\Delta\Sigma_f(r,E)\chi(E')\phi^{\dagger}(r,E')\right\} \tag{6}$$

$$\rho_d = \frac{1}{F}\left\{-\int_V \int_E dV\, dE\Delta D\,(r,E)\nabla\phi^{\dagger}(r,E)\right\} \tag{7}$$

where $\boldsymbol{F}$ is the normalization integral of the reactor given by

$$F = \int_V \int_E \int_{E'} dVdEdE'\phi(r,E)\nu\Sigma_f(r,E)\chi(E')\phi^{\dagger}(r,E') \tag{8}$$

The nomenclature is as follows: $\phi =$ forward neutron flux, $\phi^{\dagger} =$ adjoint neutron flux, $V =$ volume, $E =$ energy, $r =$ distance, $\Sigma_{a,s,f} =$ macroscopic absorption, scatter, and fission cross-section respectively, $\nu =$ neutron yield per fission, and $\chi =$ fission spectrum. Since the measurements were performed at the center of the reactor, the diffusive or leakage contribution $(\rho_d)$ goes to zero. If the sample is non-fissile, then $\rho_f$ also equals zero. This makes Eq. (3) a function of only the absorption and scatter components. Using the microscopic cross-sections and atom densities, the reactivity finally becomes:

$$\rho = \frac{NV}{F\beta}\left\{\int_{\mathrm{E}} \mathrm{dE}\sigma_a(E)\,\phi(E)\phi^{+}(E) + \int_E \int_{E'} dEdE'\sigma_s(E \rightarrow E^{'})\phi(E)[\phi^{+}\left(E^{'}\right) - \phi^{+}(E)]\right\} \tag{9}$$

The volumes, cross-sections, and atom densities are characteristics of each individual sample while the forward flux, adjoint flux, and normalization integral are functions of the entire reactor system. Because the central reactivity worths are related to a B-10, C, or H standard (i.e.

materials with well-known cross-sections), one can avoid determining the normalization integral of the reactor altogether. Accounting for the mass number of the sample, $A$, Equation (10) is used to calculate C/E values.

$$\frac{C}{E} = \frac{C_{sample} * A_{standard} * E_{standard}}{C_{standard} * A_{sample} * E_{sample}} \tag{10}$$

## 2.1 TRIPOLI-4 CODE

This section aims to only briefly present the current functionality in TRIPOLI-4 of performing exact perturbation theory calculations. More detailed and thorough discussions of Monte Carlo techniques as they apply to exact perturbation theory can be found in the references [32-36].

One can redefine the reactivity in Eq. (9), or more accurately the change in reactivity, according to exact perturbation theory as the following:

$$\Delta\rho = -\frac{\langle \phi_{ref}^{\dagger}, \left(\Delta M - \frac{\Delta P}{k_{ref}}\right) \phi_{pert} \rangle}{\langle \phi_{ref}^{\dagger}, P_{pert}\phi_{pert} \rangle} \tag{11}$$

$P$ and $M$ are the production and disappearance operators respectively, and the subscripts refer to either the perturbed or unperturbed (reference) system. Therefore, the forward neutron flux in the perturbed system (i.e. that which the sample is present in the central channel) and the adjoint neutron flux in the unperturbed system (no sample present) are needed to perform the integration over all phase space. The calculation of the forward solution is a standard process using Monte Carlo techniques, and only recently has the continuous energy adjoint solution been readily obtainable [34-37]. The approach employed in TRIPOLI-4 and others is the Iterated Fission Probability [38] method [36].

In order to solve Equation (11) exactly, and hence, perform an exact perturbation calculation, a unique three-step algorithm has been implemented in TRIPOLI-4 that is directly analogous to the deterministic approach [39]. First, the forward solution is obtained using perturbed cross-sections with the collision sites saved and parameters such as location, energy, direction, etc.…are stored. These collision sites are then used as an external source to obtain the adjoint solution with reference (unperturbed) cross-sections via the IFP method. Finally, all quantities are known to perform the continuous integration. Previous sensitivity analyses compare very well to those using deterministic approaches [36,39-41].

# 3. EXPERIMENTAL CONFIGURATION

The RRR annular driver zone consists of two concentric aluminum tanks with an inner and outer diameter of approximately 60.0 and 90.0 cm respectively. Inside the tanks are 24 rectangular fuel cassettes with 24 triangular graphite wedges sandwiched between them, all submersed in water. To aid in cooling, the graphite wedges contain a 2.2 cm hole for the water to flow. The fuel cassettes measure approximately 15 cm x 7.62 cm and contain anywhere from 8 to 12 fuel sections. Each fuel section has 6 pins that are a mixture of 60% $U_3O_8$ (20% $^{235}U$) and 40% Al by weight. The pins measure 0.737 cm in diameter and are roughly 64 cm in length.

Both of the SEG lattices are composed of aluminum[d], and the lattice used for SEG 4, 5, 7A, and 7B consists of 72 holes in a six-angular arrangement. Each of these four SEG configurations is characterized by the specific pellet, or unit cell, that fills the holes. The different unit cell arrangements are shown in Figure 3.1, and they are uniformly loaded into each respective SEG lattice. The aluminum oscillating tube filled with graphite bars inserts into the central channel. On the other hand, the SEG 6 lattice has a special radial arrangement of 4 rings, each with 12 channels that surround the central $B_4C$ absorption zone. The inner ring is filled with 36% enriched $^{235}U$ pellets, and the outer three rings are filled with natural uranium (maximum $^{238}U$ content possible). The SEG 6 central absorption zone measures 13.5 cm in diameter and contains the EK_45 or EK_10 experimental channel (5.0 and 1.2 cm in diameter, respectively). For SEG 6, the experimental channel (oscillator tube) is filled with $B_4C$. The SEG 6 lattice is seen in Figure 3.2, and Figures 3.3, 3.4, and 3.5 show the 72 hole arrangement lattice inserted into the RRR.

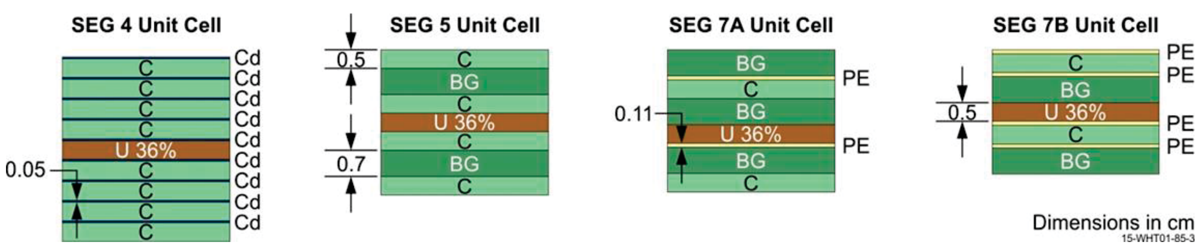


Figure 3.1. Unit cell arrangements for SEG 4, 5, 7A, and 7B

Although the system is coupled, a converter material with an inner and outer diameter measuring 48.0 and 59.0 cm, respectively, sits between the RRR and SEG zones. This helps establish an equilibrium in the central fast region. Measurements with SEG 6 used a natural uranium converter, and for the others it is graphite. The core rests on a layer of V2A steel upon an aluminum block, and above the SEG lattice sits a layer of polyethylene, cadmium, and more polyethylene.

For all experimental measurements, a given SEG lattice is loaded and then placed inside the central cavity. The annular RRR is then loaded with fuel sections to achieve a critical configuration. However, the number of fuel sections and their distribution in the driver has not been found throughout the literature. All previous analyses treat the driver region homogeneously and adjust the radius to achieve criticality. This assumption will be examined in the next section.

[d] The lattice used for SEG 1-3 and the first measurements on SEG 4 was iron.

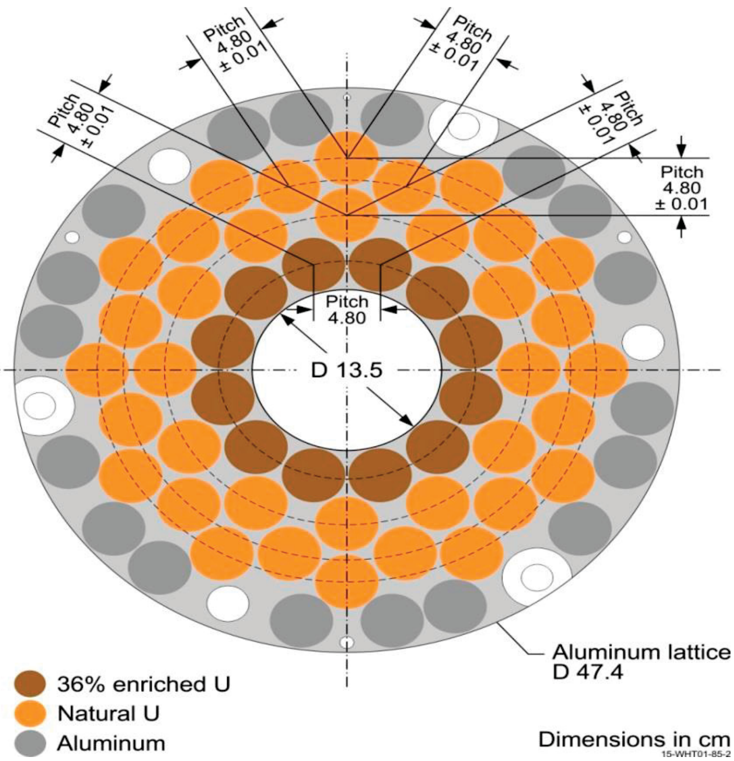


Figure 3.2. SEG 6 lattice with four concentric rings and central absorption zone.

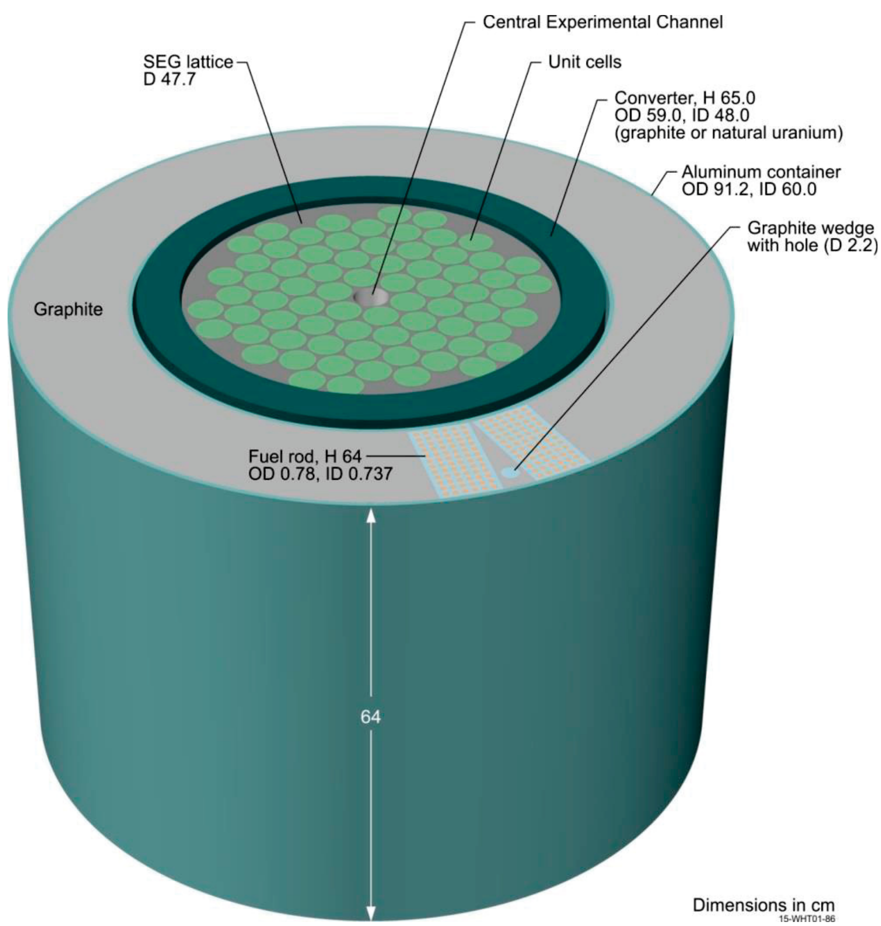


Figure 3.3. Three dimensional schematic of the RRR/SEG coupled system.

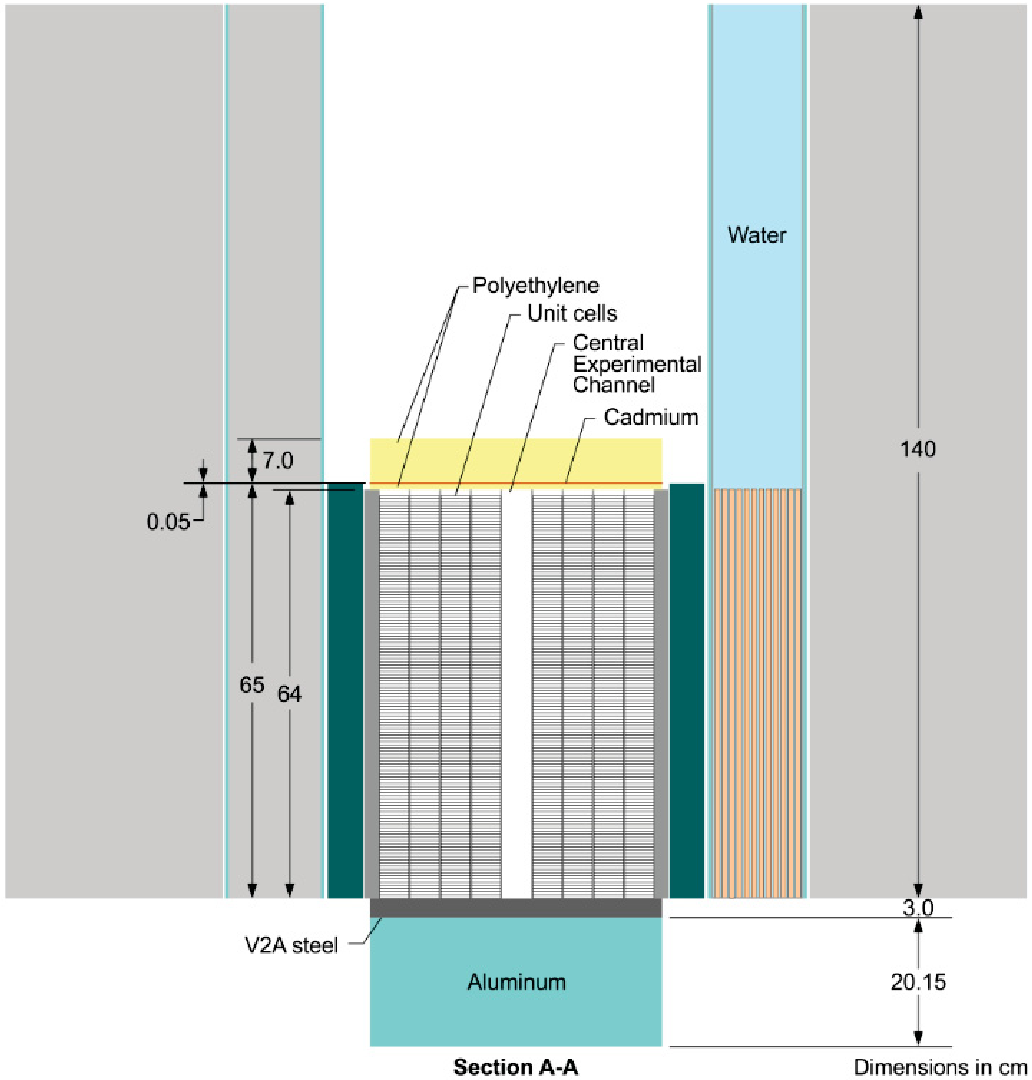


Figure 3.4. Radial view of the RRR/SEG configuration.

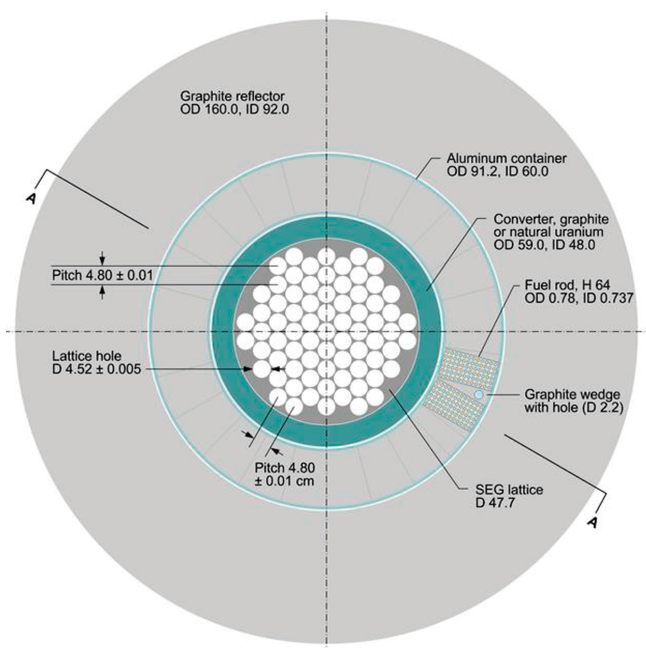


Figure 3.5. Axial view of RRR/SEG.

# 4. RESULTS

This work began with an attempt to use the direct eigenvalue differencing method in MCNP6.1. With the need to utilize exact perturbation theory, TRIPOLI-4 was employed. Comparisons are made between the different models regarding the critical size of the core and the neutron fluxes. All other results were obtained solely with TRIPOLI-4.

## 4.1 CRITICAL SIZE

The driver zone was treated both homogeneously and heterogeneously in TRIPOLI-4. The radius was adjusted in the former until a critical system was reached, and in the latter case, fuel sections consisting of 6 pins were added symmetrically[e] around the core to achieve criticality. Table 4.1 lists the eigenvalues and specifics for the critical sizes. The difference between the homogeneous models for the two codes is very respectable, all less than 80 pcm. This is likely attributed to subtle differences in the inner workings of the codes. The critical radii for prior analysis has only been found for that involving the JEF-2/ERANOS/ECCO scheme; for SEG 4, 5, and 6 the radii are 7.14 , 6.21, and 8.55 cm respectively [16, 17, 18]. The different cross-section libraries more than likely account for the bulk of the differences.

Table 4.1. Critical characteristics for the different SEG lattices.

| | SEG 4 | SEG 5 | SEG 6 EK_45 | SEG 7A | SEG7B |
|---|---|---|---|---|---|
| | $k_{eff}$ | | | | |
| **MCNP6/1.1 ENDF/B-7.0** | 1.00058 | 0.99954 | 1.00040 | 1.00001 | 1.00060 |
| **ENDF/B-7.1** | 0.99943 | 0.99867 | 0.99961 | 0.99918 | 0.99982 |
| **TRIPOLI-4 ENDF/B-7.1 (homogeneous)** | 0.99989 | 0.99920 | 1.00036 | 0.99979 | 1.00024 |
| **TRIPOLI-4 ENDF/B-7.1 (heterogeneous)** | 0.99848 | 1.00034 | 0.99905 | 0.99952 | 1.00105 |
| | $\mathbf{0.00001 < 1\sigma < 0.00004}$ | | | | |
| **$\Delta k_{eff}$ for ENDF/B-7.1 Homogeneous (pcm)** | 46 | 53 | 75 | 61 | 42 |
| **Homogeneous Critical Radius (cm)** | 7.82 | 7.45 | 9.17 | 8.50 | 7.98 |
| **Heterogeneous Critical # Fuel Plates[f]** | 141 | ~ 138 | ~ 158 | 150 | ~ 145 |

[e] Symmetry was assumed but may not have been the case. As seen in Figure A.1 in Appendix A, the distribution of driver fuel does not appear to be symmetric.

[f] SEG 5, 6, and 7B each have one driver fuel plate that contains less than 6 pins. It is unknown whether the number of fuel pins could actually be less than 6, but this was merely done to get an eigenvalue as close to unity as possible.

## 4.2 NEUTRON FLUX

The normalized forward and adjoint fluxes in the central channel were characterized using TRIPOLI4 with the driver zone treated both homogeneously and heterogeneously. These are shown in Figures 4.1 – 4.5 along with data from previous analyses using the deterministic route JEF/ERANOS/ECCO and the initial MCNP analysis. Figures 4.6 – 4.10 and 4.11 – 4.15 compare individually the forward and adjoint fluxes between the homogeneous and heterogeneous cases on a linear scale[g]. The fluxes differ by less than 1.0% (in fact they nearly completely lie on top of each other), thus the homogeneous treatment of the driver zone is deemed acceptable. The ABBN 26 energy group structure was used for all comparisons since this was used in the previous analyses. As expected, the importance function for SEG 4, 5, 7A, and 7B is flat and energy independent, while SEG 6 has a monotonically rising importance function. SEG 7A and 7B are also seen to have much softer spectrums than the others due to the polyethylene present in the unit cells.

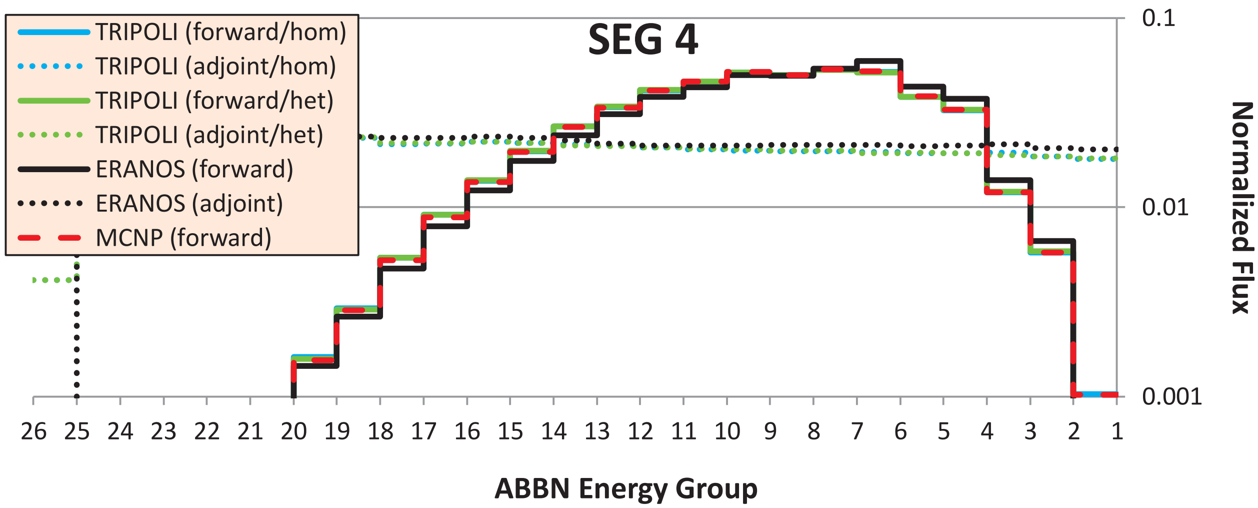


Figure 4.1. SEG 4 forward and adjoint flux.

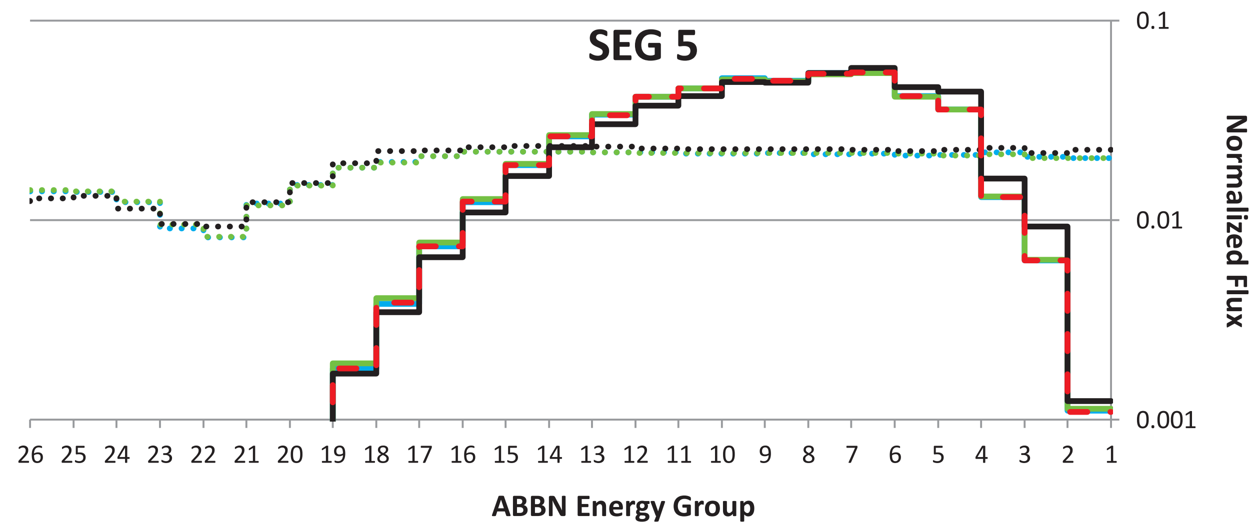


Figure 4.2. SEG 5 forward and adjoint fluxes.

[g] Error bars are present on the Monte Carlo (TRIPOLI) calculations, they are just too small to observe.

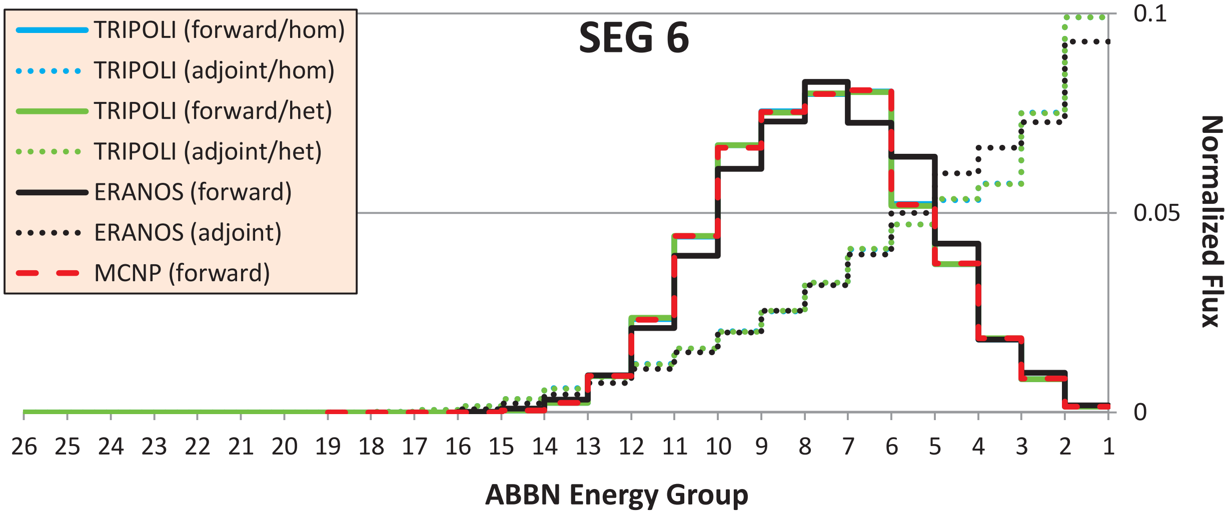


Figure 4.3. SEG 6 EK_45 forward and adjoint fluxes.

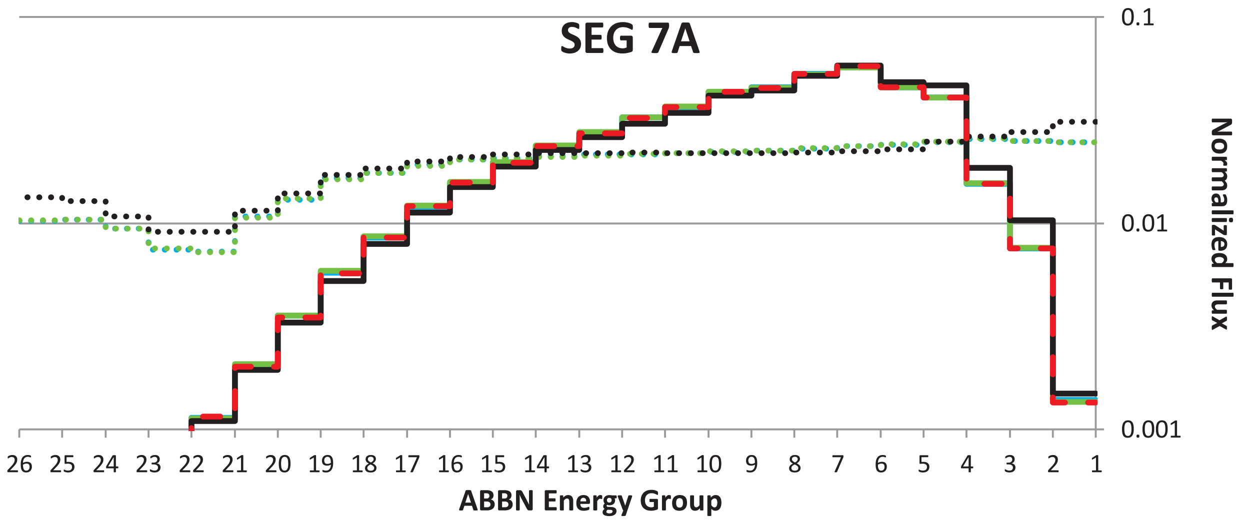


Figure 4.4. SEG 7A forward and adjoint fluxes.

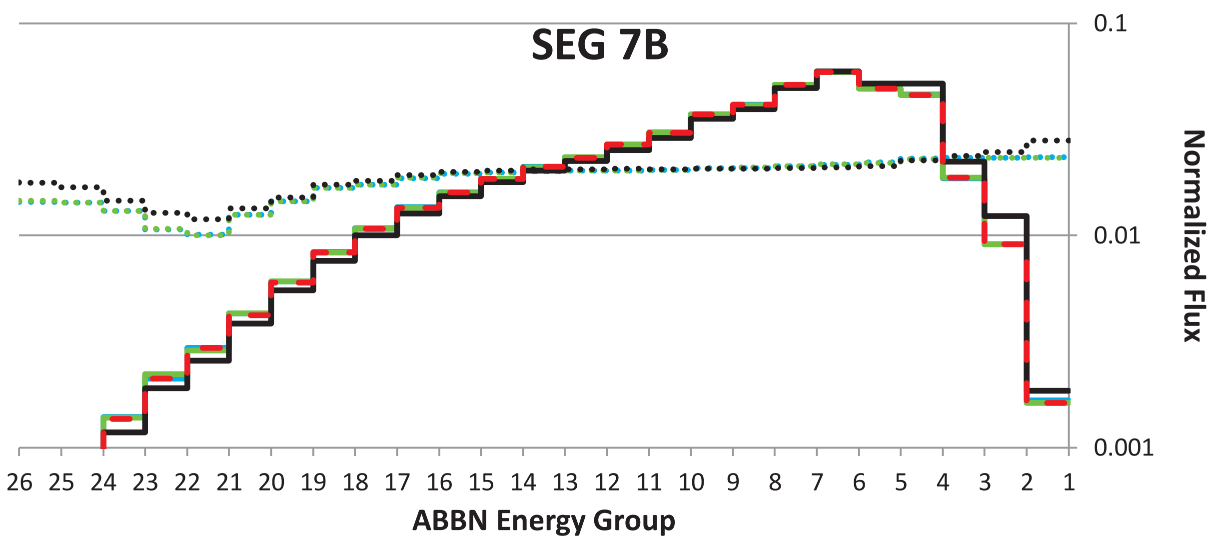


Figure 4.5. SEG 7B forward and adjoint fluxes.

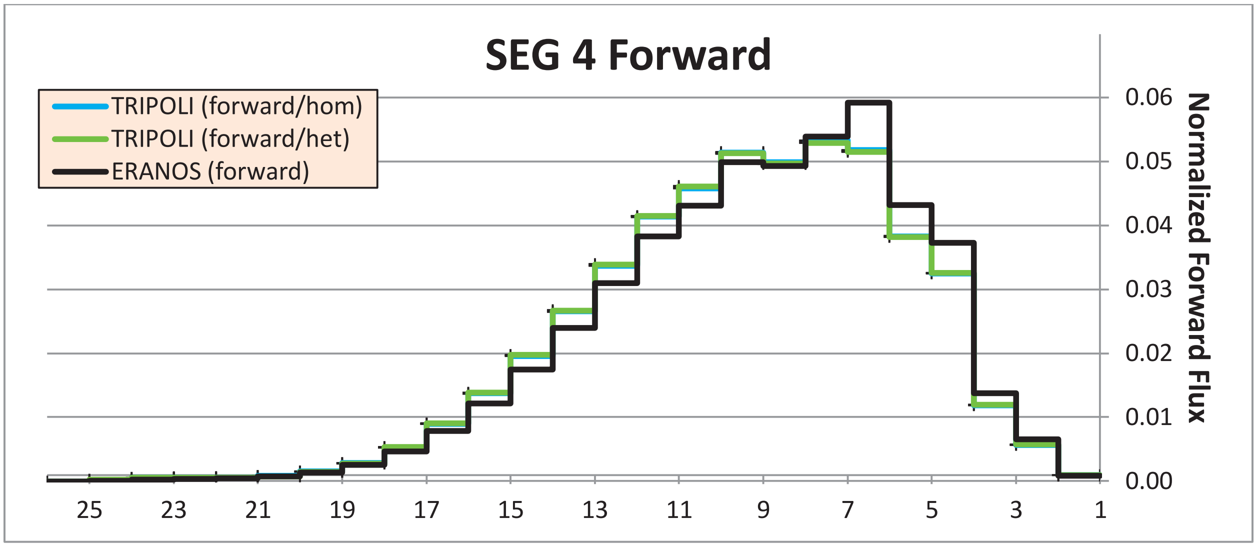

Figure 4.6. Linear plot of SEG 4 normalized forward flux.

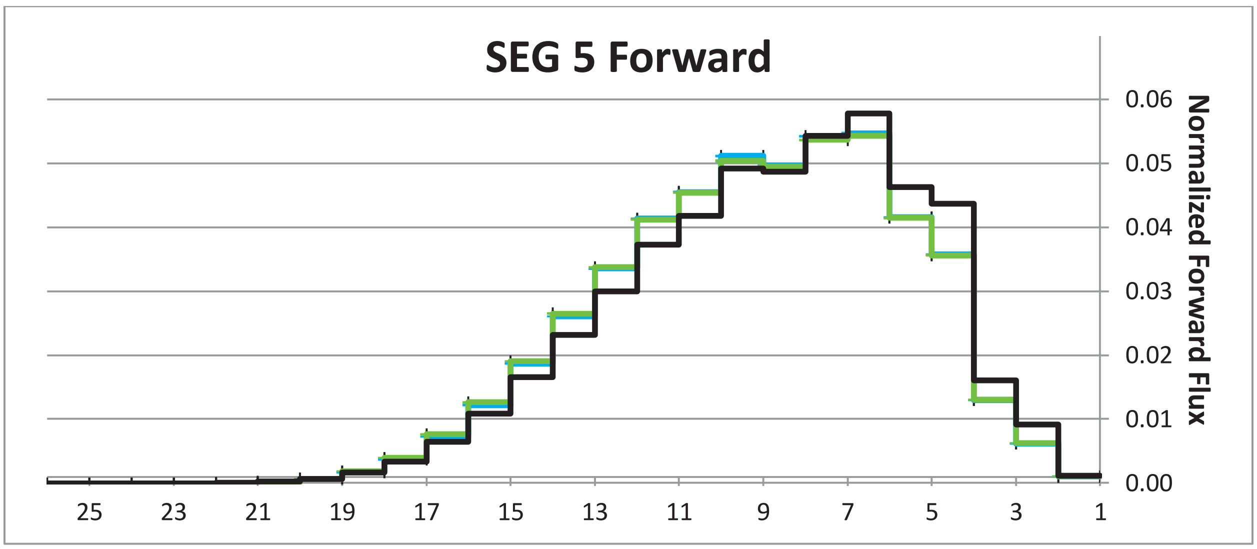

Figure 4.7. Linear plot of SEG 5 normalized forward flux.

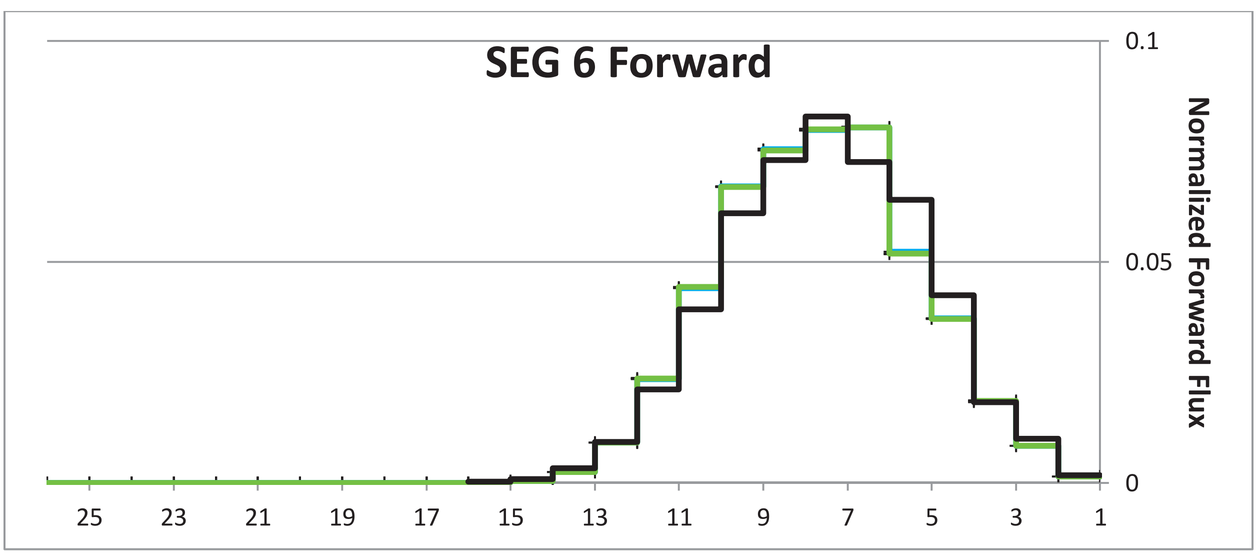

Figure 4.8. Linear plot of SEG 6 EK_45 normalized forward flux.

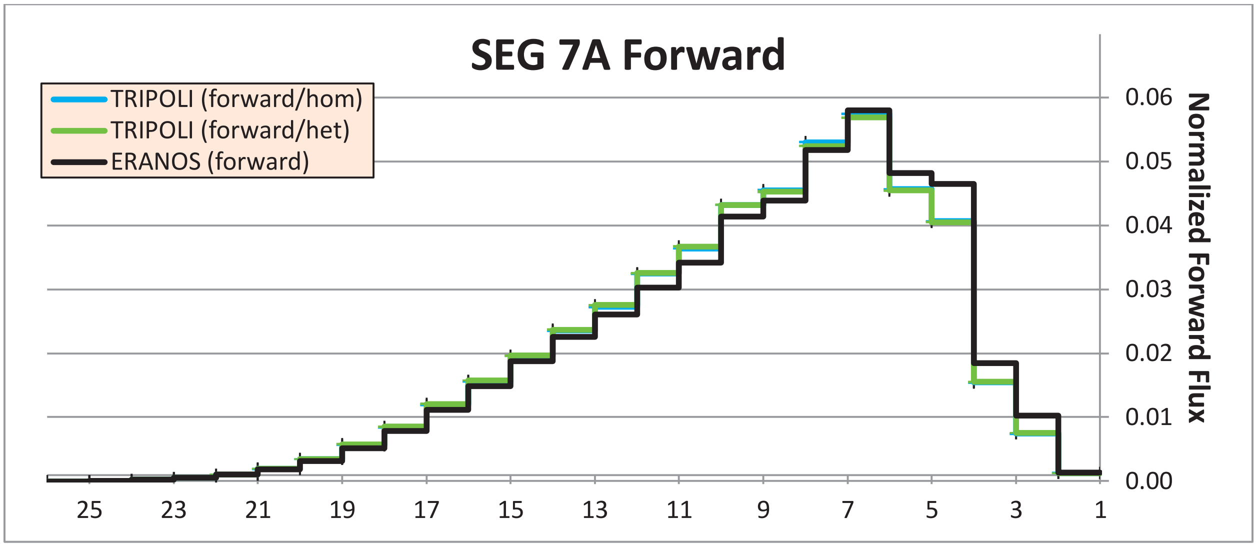


Figure 4.9. Linear plot of SEG 7A normalized forward flux.

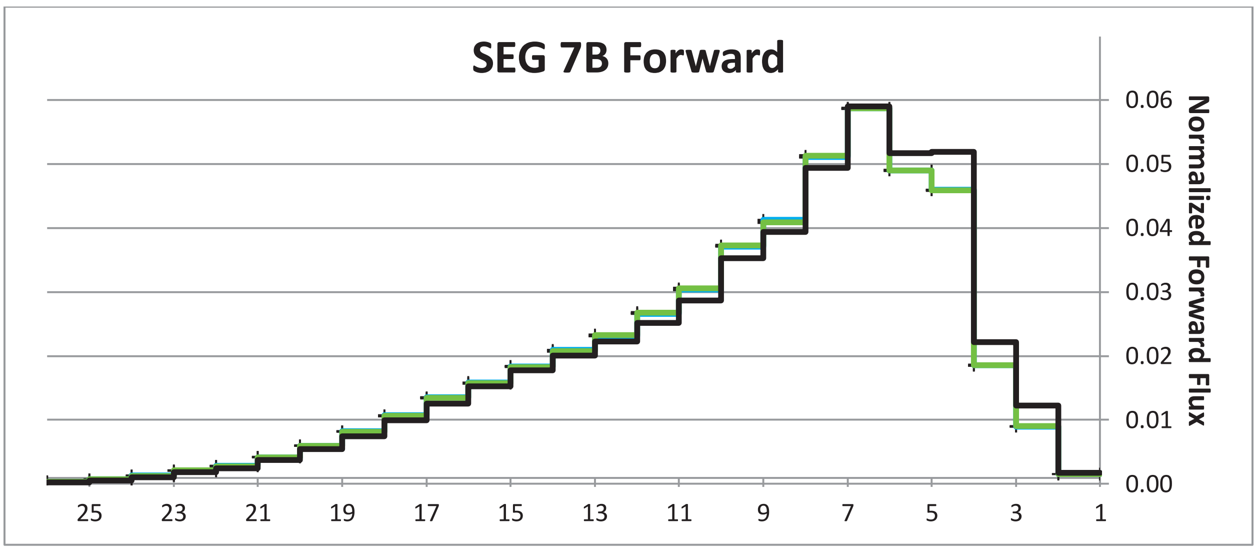


Figure 4.10. Linear plot of SEG 7B normalized forward flux.

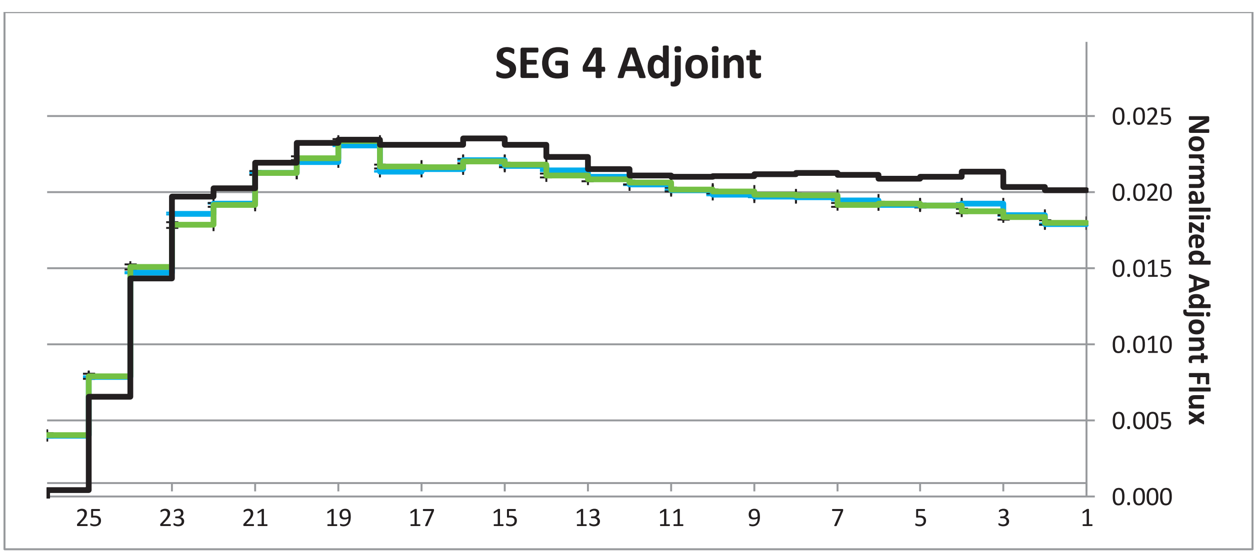


Figure 4.11. Linear plot of SEG 4 normalized adjoint flux.

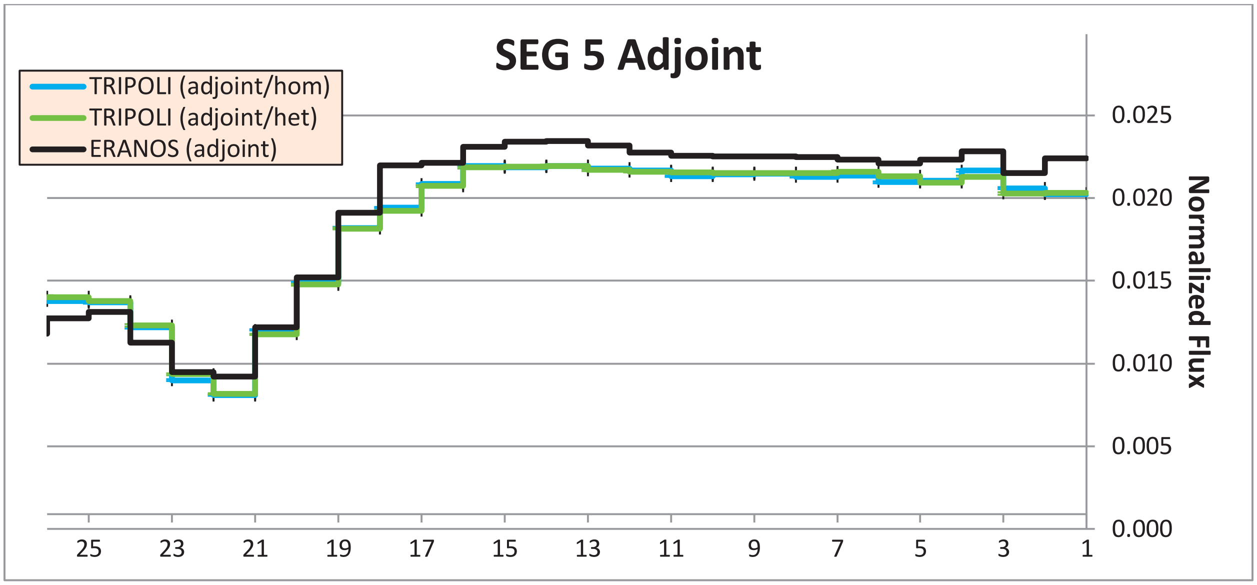


Figure 4.12. Linear plot of SEG 5 normalized adjoint flux.

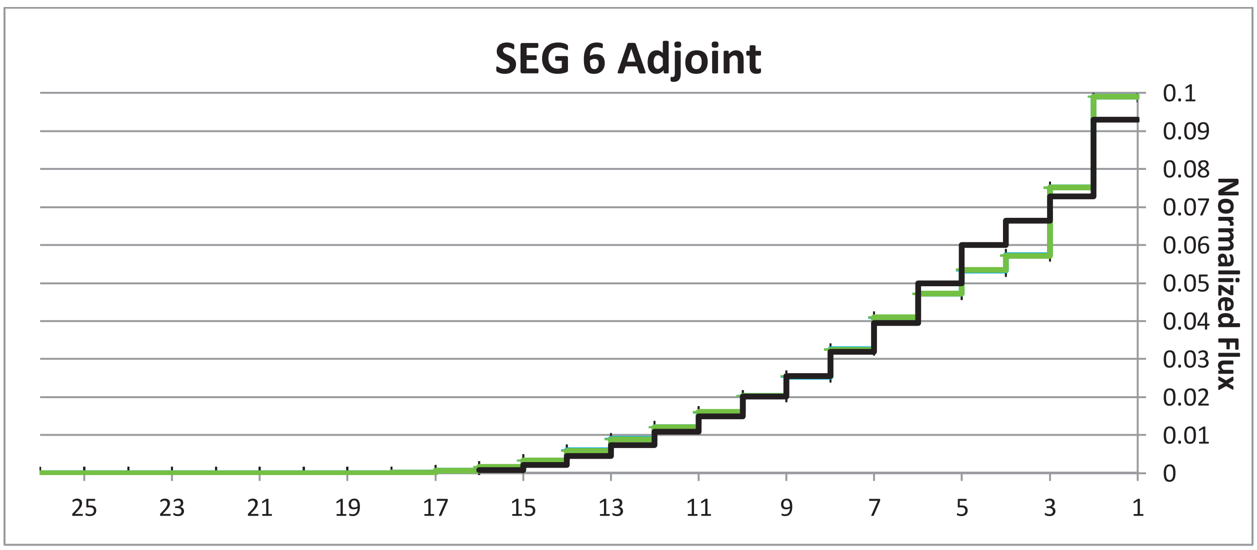


Figure 4.13. Linear plot of SEG 6 EK_45 normalized adjoint flux.

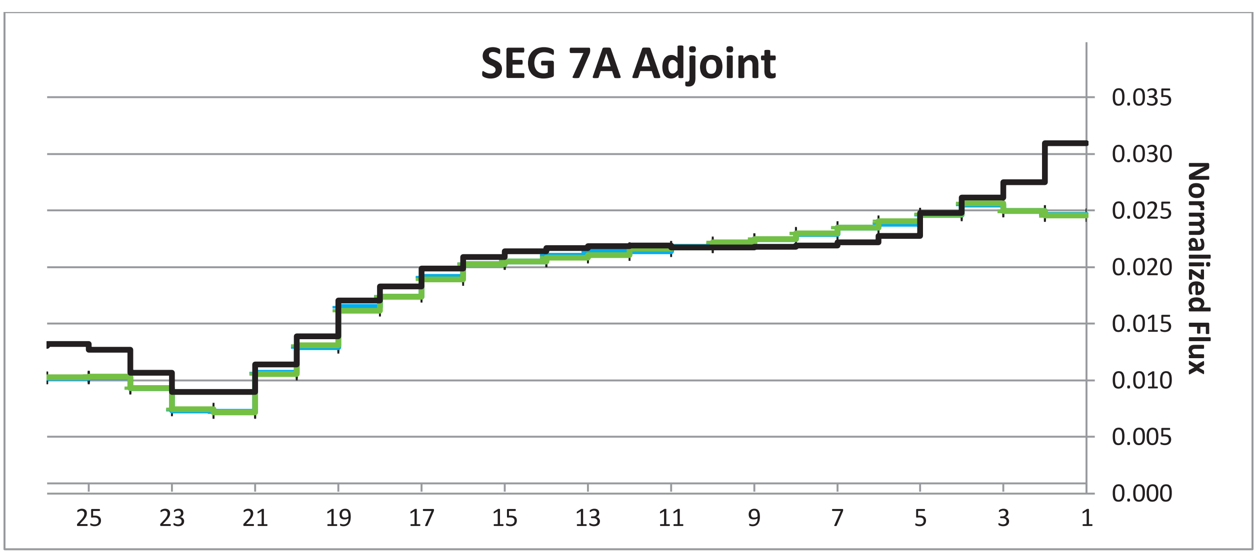


Figure 4.14. Linear plot of SEG 7A normalized adjoint flux.

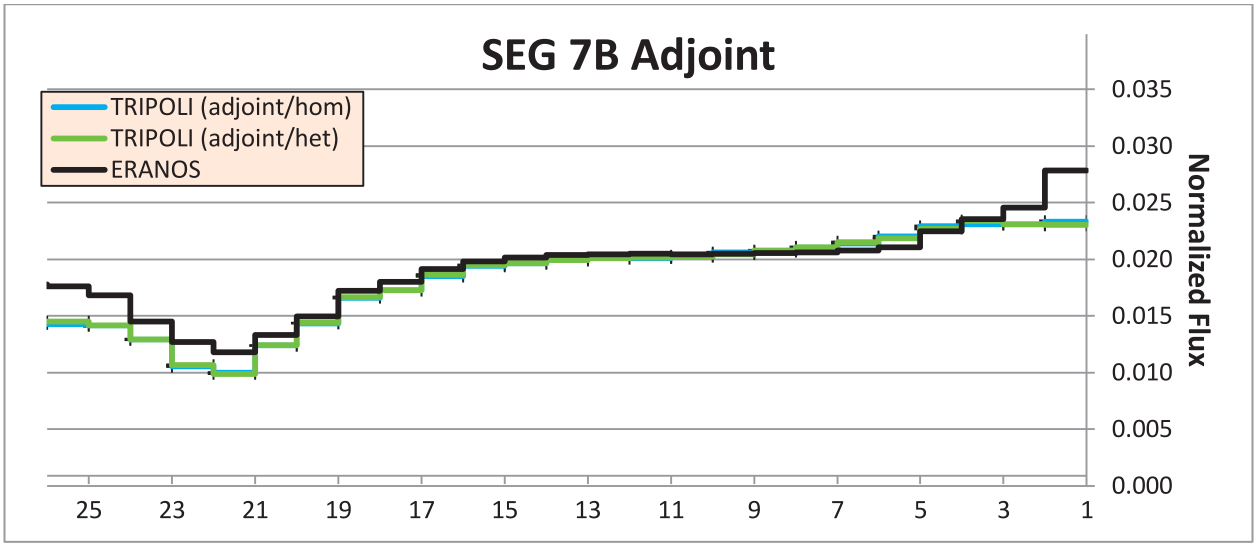

Figure 4.15. Linear plot of SEG 7B normalized adjoint flux.

## 4.3 CRW MEASUREMENTS AND C/E VALUES

Having characterized the forward and adjoint spectrums, the EPT capability in TRIPOLI4 was used to determine the central reactivity worth (CRW) of the different samples. Although TRIPOLI4 is a continuous energy code, the CRW values were calculated using forward and adjoint fluxes that were both CE and discrete in energy. This was done because there is an unresolved bug in the code that yields incorrect results when using CE for sensitivity analysis[h]. Thus the energy groups used were a 1968 fine group and a 33 coarse group structure. Both the JEFF-3.2 and ENDF-B/VII.I[i] neutron cross-section libraries were used. C/E values are given using the 1968g structure in Tables 4.2 – 4.6 along with the most recently calculated C/E values from previous analyses. These most recent previous analyses come from both the European route, JEF-2.2/ERANOS/ECCO, and the Japanese route, JENDL-3.2/SLAROM/CITATION/PERKY [7, 15]. Values that differ from unity by more than 5% of the total C/E error are highlighted. The CRW values calculated for SEG 4, 5, and 7A are all related to B-10, and the SEG 6 EK_45 CRW values are related to both C and H (both being nearly pure scatterers). Two different B-10 measurements were made for SEG 5; one for structural materials and one for fission products.

In addition to the C/E values, Tables 4.7 – 4.9 give the percent of the reactivity change broken down by the elastic, inelastic, and scattering contributions[j] for SEG 5, 7A, and 6 EK_45, respectively. Since the importance function is nearly energy independent for SEG 5, the reactivity contribution due to scattering for most samples is only around 1% or less (and this includes taking into account a 1 sigma deviation, despite the large calculated errors). Contributions larger than 5% are highlighted. SEG 7A, with its similar but softer spectrum, yields comparable results. Due to the monotonically rising importance function characteristic of SEG 6, the inelastic component tends to be the largest contributor to the reactivity effect.

---

[h] Personal communication with Pierre Leconte (pierre.leconte@cea.fr).

[i] For unknown reasons the ENDF-7.1 cross section libraries for europium and tungsten could not be utilized.

[j] The contribution from fission is included for U-235, U-238, and Th-232.

Table 4.2. C/E values related to B-10 for SEG 4 using JEFF-3.2 and ENDF-7.1 libraries.

| Sample Material | ID No. | Exp. CRW (mc/g) | Exp. Err (%) | C/E 70g JNC JENDL -3.2 | C/E 70g JNC JEF-2.2 | C/E 33g Eur. JEF-2.2 | C/E 1968g TRIPOLI JEFF-3.2 | Calc. Err. (%) | Tot. C/E Err. (%) | C/E 1968g TRIPOLI ENDF-7.1 | Calc. Err. (%) | Tot. C/E Err. (%) |
|---|---|---|---|---|---|---|---|---|---|---|---|---|
| B-10 | 105 | - 1326 ± 20 | 2 | 1.000 | 1.000 | 1.000 | 1.000 | 0.6 | 2.1 | 1.000 | 0.424 | 2.0 |
| U-235 | 925 | + 31.2 ± 2.0 | 10 | 0.950 | 0.980 | 0.965 | **-0.741** | 0.6 | 10.0 | **-0.726** | 0.411 | 10.0 |
| U-238 | 928 | - 7.2 ± 0.5 | 10 | **1.260** | **1.242** | 1.056 | **1.174** | 4.0 | 10.8 | **1.280** | 3.457 | 10.6 |
| Ta | 731 | - 37.0 ± 2.0 | 8 | 0.922 | 0.884 | **0.851** | 0.956 | 2.3 | 8.3 | 0.988 | 1.782 | 8.2 |
| Mo | 42 | - 6.2 ± 0.5 | 12 | **1.208** | 1.153 | 0.906 | 1.135 | 3.9 | 12.6 | 1.154 | 2.552 | 12.3 |
| Nb | 413 | - 8.5 ± 0.5 | 10 | 1.039 | 1.049 | 0.889 | 0.966 | 1.2 | 10.1 | 0.937 | 0.867 | 10.0 |
| Mn | 25 | - 8.3 ± 0.6 | 11 | **0.826** | **1.214** | 0.957 | **1.170** | 2.6 | 11.3 | **0.835** | 1.973 | 11.2 |
| Fe | 26 | - 0.52 ± 0.07 | 12 | **1.340** | **1.388** | 1.086 | **0.774** | 6.1 | 13.4 | **0.819** | 3.884 | 12.6 |
| Cr | 24 | - 0.50 ± 0.03 | 10 | **1.167** | **1.291** | 1.076 | **0.733** | 5.2 | 11.3 | 0.943 | 2.664 | 10.3 |
| Ni | 28 | - 1.00 ± 0.08 | 11 | 1.067 | 1.104 | 1.091 | 1.007 | 2.2 | 11.2 | 0.867 | 1.702 | 11.1 |
| Cd | 48 | - 7.5 ± 0.5 | 10 | **1.296** | **1.502** | 1.046 | 1.138 | 2.5 | 10.3 | 1.151 | 1.781 | 10.2 |
| Cu | 29 | - 4.2 ± 0.3 | 11 | 1.030 | 1.093 | 0.878 | 0.854 | 3.1 | 11.4 | 0.843 | 2.037 | 11.2 |
| Zr | 40 | - 0.90 ± 0.08 | 12 | **1.192** | 1.051 | 0.911 | 0.884 | 3.4 | 12.5 | 1.067 | 2.255 | 12.2 |
| W | 74 | - 15.0 ± 1.0 | 10 | **0.823** | 0.876 | 0.896 | 1.029 | 5.0 | 11.2 | - | - | - |
| Mo-95 | 425 | - 18.0 ± 1.0 | 10 | 1.121 | **1.151** | 0.913 | 1.068 | 5.2 | 11.3 | 1.044 | 3.157 | 10.5 |
| Mo-97 | 427 | - 11.0 ± 0.5 | 9 | 1.106 | **1.142** | 0.952 | 1.024 | 1.3 | 9.1 | 0.996 | 0.969 | 9.1 |
| Mo-98 | 428 | - 5.3 ± 0.4 | 12 | 0.856 | 0.891 | **0.773** | **0.693** | 2.4 | 12.2 | **0.815** | 1.930 | 12.2 |
| Mo-100 | 420 | - 3.5 ± 0.3 | 13 | 0.995 | 0.966 | **0.803** | 0.906 | 2.8 | 13.3 | 0.930 | 2.231 | 13.2 |
| Rh-103 | 453 | - 35.0 ± 3.0 | 12 | 1.096 | 1.132 | 1.056 | 1.077 | 2.3 | 12.2 | 1.060 | 1.603 | 12.1 |
| Pd-105 | 465 | - 30.5 ± 5.0 | 19 | 1.031 | 1.013 | 0.882 | 0.942 | 0.9 | 19.0 | 0.937 | 0.694 | 19.0 |
| Ag-109 | 479 | - 65.0 ± 5.0 | 12 | **0.777** | 0.846 | **0.809** | 1.027 | 4.8 | 12.9 | 0.948 | 3.778 | 12.6 |
| Cs-133 | 553 | - 22.0 ± 2.0 | 13 | 1.000 | 0.985 | 1.038 | 1.138 | 2.9 | 13.3 | 1.030 | 2.130 | 13.2 |
| Sm-149 | 629 | - 105 ± 5.0 | 9 | 1.057 | 1.137 | 1.094 | 1.098 | 1.3 | 9.1 | 1.097 | 1.025 | 9.1 |
| Eu-153 | 633 | - 93.0 ± 5.0 | 10 | 1.009 | 0.992 | 1.108 | 1.014 | 1.0 | 10.0 | - | - | - |

Table 4.3. C/E values related to B-10 for SEG 5 using JEFF-3.2 and ENDF-7.1 libraries.

| Sample Material | ID No. | Exp. CRW (mc/g) | Exp. Err (%) | C/E 70g JNC JENDL -3.2 | C/E 70g JNC JEF-2.2 | C/E 33g Eur. JEF-2.2 | C/E 1968g TRIPOLI JEFF-3.2 | Calc. Err. (%) | Tot. C/E Err. (%) | C/E 1968g TRIPOLI ENDF-7.1 | Calc. Err. (%) | Tot. C/E Err. (%) |
|---|---|---|---|---|---|---|---|---|---|---|---|---|
| B-10 ss | 105 | - 1230 ± 20 | 2 | 1.000 | 1.000 | 1.000 | 1.000 | 0.4 | 2.0 | 1.000 | 0.3 | 2.0 |
| Ta | 731 | - 31.5 ± 1.0 | 7 | 0.956 | 0.933 | 0.956 | 0.932 | 0.8 | 7.0 | 0.999 | 0.8 | 7.0 |
| U-235 | 925 | + 31.2 ± 2.0 | 10 | 1.138 | 1.124 | 1.084 | **1.179** | 0.3 | 10.0 | **1.176** | 0.3 | 10.0 |
| Mo | 42 | - 7.4 ± 0.5 | 10 | 1.031 | 0.984 | 0.964 | 1.056 | 2.2 | 10.2 | 1.108 | 2.3 | 10.3 |
| Mn | 25 | - 12.0 ± 0.5 | 7 | **0.658** | 0.942 | 0.952 | 0.904 | 1.3 | 7.1 | 1.002 | 2.1 | 7.3 |
| Cd | 48 | - 10.0 ± 0.5 | 9 | 1.070 | **1.214** | **1.215** | 1.102 | 2.4 | 9.3 | **1.173** | 2.6 | 9.4 |
| Nb | 413 | - 10.0 ± 0.6 | 9 | 1.072 | 1.048 | 1.022 | **1.148** | 0.8 | 9.0 | **1.155** | 0.8 | 9.0 |
| Cu | 29 | - 4.5 ± 0.5 | 14 | 1.174 | **1.214** | 1.119 | 0.997 | 1.9 | 14.1 | 1.179 | 1.8 | 14.1 |
| Zr | 40 | - 1.05 ± 0.1 | 13 | **1.302** | 1.085 | 1.032 | **1.210** | 2.1 | 13.2 | **1.334** | 1.8 | 13.1 |
| W | 74 | - 10.0 ± 0.5 | 8 | 0.918 | 1.019 | 1.085 | 1.002 | 2.7 | 8.5 | - | - | - |
| Fe | 26 | - 0.7 ± 0.06 | 11 | **1.342** | **1.232** | 1.084 | 1.062 | 3.1 | 11.4 | **1.246** | 2.8 | 11.3 |

| | | | | | | | | | | | | |
|---|---|---|---|---|---|---|---|---|---|---|---|---|
| Cr | 24 | - 0.8 ± 0.06 | 10 | 1.037 | 1.095 | 1.032 | **0.840** | 2.4 | 10.3 | **0.828** | 2.3 | 10.3 |
| Ni | 28 | - 1.3 ± 0.1 | 10 | **1.237** | **1.185** | 1.073 | **1.380** | 5.7 | 11.5 | **1.213** | 1.0 | 10.1 |
| Co | 279 | - 20.0 ± 1.5 | 10 | 1.032 | 1.076 | 0.992 | **1.165** | 2.6 | 10.3 | **1.252** | 2.7 | 10.4 |
| B-10 fp | 105 | - 1174 ± 20 | 2 | 1.000 | 1.000 | 1.000 | 1.000 | 0.4 | 2.0 | 1.000 | 0.3 | 2.0 |
| Mo-95 | 425 | - 14.5 ± 1.0 | 10 | **1.185** | **1.194** | 1.133 | 1.148 | 2.9 | 10.4 | **1.256** | 3.0 | 10.4 |
| Mo-97 | 427 | - 14.0 ± 1.0 | 10 | 0.980 | 0.994 | 0.954 | 0.950 | 0.8 | 10.0 | 0.962 | 0.8 | 10.0 |
| Mo-98 | 428 | - 5.0 ± 0.6 | 15 | 1.035 | 1.039 | 1.061 | 0.961 | 1.7 | 15.1 | 1.027 | 1.9 | 15.1 |
| Mo-100 | 420 | - 4.1 ± 0.5 | 16 | 0.996 | 0.923 | 0.888 | 0.983 | 2.2 | 16.1 | 0.951 | 2.0 | 16.1 |
| Rh-103 | 453 | - 27.0 ± 1.0 | 7 | 0.899 | 0.914 | 0.901 | 0.888 | 0.8 | 7.0 | **0.847** | 0.7 | 7.0 |
| Pd-105 | 465 | - 30.2 ± 1.0 | 7 | 1.117 | 1.077 | 1.064 | 1.058 | 0.5 | 7.0 | 1.057 | 0.5 | 7.0 |
| Ag-109 | 479 | - 31.5 ± 1.5 | 8 | 0.886 | 0.926 | 0.929 | 0.937 | 1.2 | 8.1 | 0.888 | 1.5 | 8.1 |
| Cs-133 | 553 | - 19.5 ± 2.0 | 13 | 0.909 | 0.912 | 0.926 | 0.942 | 1.1 | 13.0 | 0.896 | 1.1 | 13.0 |
| Nd-143 | 603 | - 16.0 ± 1.0 | 9 | 0.882 | 0.897 | 0.896 | 0.865 | 1.3 | 9.1 | **0.776** | 1.3 | 9.1 |
| Nd-145 | 605 | - 18.0 ± 1.0 | 9 | 1.020 | 1.018 | 1.066 | 0.972 | 0.9 | 9.0 | 0.930 | 1.2 | 9.1 |
| Sm-149 | 629 | - 83 ± 5 | 9 | 1.023 | 1.121 | **1.191** | 1.105 | 1.9 | 9.2 | 1.097 | 2.3 | 9.3 |
| Eu-153 | 633 | - 75 ± 5 | 10 | 1.059 | 1.068 | 1.091 | 1.040 | 0.4 | 10.0 | - | - | - |

Table 4.4. C/E values related to H for SEG 6 EK_45 using JEFF-3.2 and ENDF-7.1 libraries.

| Sample Material | ID No. | Exp. CRW (mc/g) | Exp. Err (%) | C/E 70g JNC JENDL -3.2 | C/E 70g JNC JEF-2.2 | C/E 1968g TRIPOLI JEFF-3.2 | Calc. Err. (%) | Tot. C/E Err. (%) | C/E 1968g TRIPOLI ENDF-7.1 | Calc. Err. (%) | Tot. C/E Err. (%) |
|---|---|---|---|---|---|---|---|---|---|---|---|
| H | 1 | - 1099 ± 10 | 5 | 1.000 | 1.000 | 1.000 | 0.2 | 5.0 | 1.000 | 0.2 | 5.0 |
| C | 6 | - 7.35 ± 0.06 | 8 | 0.918 | 0.959 | 1.041 | 0.2 | 8.0 | 1.053 | 0.2 | 8.0 |
| B-10 | 105 | - 95.9 ± 6.0 | 12 | **0.823** | **0.821** | **0.771** | 0.2 | 12.0 | **0.771** | 0.2 | 12.0 |
| Mo | 42 | - 1.70 ± 0.04 | 7 | 0.935 | 0.898 | 0.960 | 0.3 | 7.0 | 0.995 | 0.3 | 7.0 |
| Fe | 26 | - 1.22 ± 0.04 | 7 | 0.925 | 0.952 | 0.923 | 0.3 | 7.0 | 0.948 | 0.6 | 7.0 |
| Cr | 24 | - 1.21 ± 0.04 | 7 | 0.887 | 0.977 | 1.014 | 0.4 | 7.0 | 1.046 | 0.4 | 7.0 |
| Ni | 28 | - 1.55 ± 0.05 | 9 | 0.986 | 1.096 | 0.984 | 0.4 | 9.0 | 0.996 | 0.2 | 9.0 |
| Al | 13 | - 2.00 ± 0.06 | 8 | 1.109 | **1.202** | **1.152** | 0.3 | 8.0 | **1.148** | 0.3 | 8.0 |
| Zr | 40 | - 1.01 ± 0.03 | 8 | 0.918 | **0.859** | 1.003 | 0.3 | 8.0 | 0.949 | 0.2 | 8.0 |
| Ti | 22 | - 1.93 ± 0.05 | 8 | 0.911 | 0.881 | - | - | - | - | - | - |
| Cd | 48 | - 1.89 ± 0.05 | 7 | **0.802** | 1.026 | 0.993 | 0.3 | 7.0 | 1.004 | 0.3 | 7.0 |
| Pb | 82 | - 0.32 ± 0.02 | 12 | 1.166 | 0.883 | 0.882 | 0.4 | 12.0 | 0.902 | 0.4 | 12.0 |
| Bi | 839 | - 0.30 ± 0.02 | 12 | 0.911 | 0.986 | 0.933 | 0.4 | 12.0 | 0.949 | 0.4 | 12.0 |
| Mg | 12 | - 3.01 ± 0.08 | 13 | 1.082 | 1.014 | **1.181** | 0.3 | 13.0 | 1.169 | 0.3 | 13.0 |
| Be | 4 | - 14.04 ± 0.10 | 7 | **1.186** | **1.138** | 1.090 | 0.2 | 7.0 | 1.113 | 0.2 | 7.0 |
| W | 74 | - 1.34 ± 0.03 | 9 | 0.926 | 0.912 | 0.913 | 0.3 | 9.0 | - | - | - |
| Cu | 29 | - 1.45 ± 0.02 | 8 | 1.046 | 1.063 | 1.007 | 0.3 | 8.0 | 1.032 | 0.3 | 8.0 |
| Au | 79 | -1.63 ± 0.07 | 9 | | 0.919 | 0.895 | 0.3 | 9.0 | - | - | - |
| Mn | 25 | - 1.53 ± 0.03 | 8 | 0.896 | 1.045 | 1.087 | 0.5 | 8.0 | **1.214** | 0.3 | 8.0 |
| Ta | 731 | - 2.15 ± 0.02 | 7 | **0.874** | **0.834** | **0.771** | 0.3 | 7.0 | **0.878** | 0.3 | 7.0 |
| V | 23 | - 1.91 ± 0.05 | 9 | 0.934 | 1.034 | 0.974 | 0.5 | 9.0 | 1.006 | 0.3 | 9.0 |
| Si | 14 | - 1.82 ± 0.09 | 11 | 0.893 | 1.049 | 1.007 | 0.3 | 11.0 | 1.067 | 0.3 | 11.0 |
| Nb | 413 | - 1.96 ± 0.04 | 8 | 0.943 | 0.900 | 0.886 | 0.3 | 8.0 | 0.910 | 0.3 | 8.0 |
| Co | 279 | - 1.25 ± 0.02 | 8 | 1.119 | **1.184** | **1.219** | 0.4 | 8.0 | **1.262** | 0.3 | 8.0 |
| U-235 | 925 | + 10.9 ± 0.07 | 7 | 0.898 | 0.907 | 0.963 | 0.2 | 7.0 | 0.975 | 0.3 | 7.0 |
| U-238 | 928 | - 0.703 ± 0.04 | 12 | 0.906 | 0.881 | 0.989 | 0.3 | 12.0 | 0.999 | 0.3 | 12.0 |
| Th | 902 | - 1.35 ± 0.04 | 9 | **0.858** | **0.832** | 0.867 | 0.3 | 9.0 | 0.892 | 0.4 | 9.0 |

Table 4.5. C/E values related to C for SEG 6 EK_45 using JEFF-3.2 and ENDF-7.1 libraries.

| Sample Material | ID No. | Exp. CRW (mc/g) | Exp. Err (%) | C/E 33g Eur. JEF-2.2 | C/E 1968g TRIPOLI JEFF-3.2 | Calc. Err. (%) | Tot. C/E Err. (%) | C/E 1968g TRIPOLI ENDF-7.1 | Calc. Err. (%) | Tot. C/E Err. (%) |
|---|---|---|---|---|---|---|---|---|---|---|
| H | 1 | - 1099 ± 10 | 5 | 1.071 | 0.960 | 0.2 | 5.0 | 0.950 | 0.7 | 5.1 |
| C | 6 | - 7.35 ± 0.06 | 8 | 1.000 | 1.000 | 0.2 | 8.0 | 1.000 | 31.7 | 32.7 |
| B-10 | 105 | - 95.9 ± 6.0 | 12 | 0.896 | **0.741** | **0.2** | 12.0 | **0.732** | 0.3 | 12.0 |
| Mo | 42 | - 1.70 ± 0.04 | 7 | 0.913 | 0.922 | 0.3 | 7.0 | 0.945 | 2.3 | 7.4 |
| Fe | 26 | - 1.22 ± 0.04 | 7 | 0.916 | 0.886 | 0.3 | 7.0 | 0.900 | 2.8 | 7.5 |
| Cr | 24 | - 1.21 ± 0.04 | 7 | 0.915 | 0.974 | 0.4 | 7.0 | 0.993 | 2.3 | 7.4 |
| Ni | 28 | - 1.55 ± 0.05 | 9 | 1.133 | 0.945 | 0.4 | 9.0 | 0.946 | 1.0 | 9.1 |
| Al | 13 | - 2.00 ± 0.06 | 8 | 1.032 | 1.106 | 0.3 | 8.0 | 1.091 | 2.2 | 8.3 |
| Zr | 40 | - 1.01 ± 0.03 | 8 | **0.860** | 0.963 | 0.3 | 8.0 | 0.902 | 1.8 | 8.2 |
| Ti | 22 | - 1.93 ± 0.05 | 8 | 0.921 | - | - | - | - | - | - |
| Cd | 48 | - 1.89 ± 0.05 | 7 | 1.105 | 0.954 | 0.3 | 7.0 | 0.953 | 2.6 | 7.5 |
| Pb | 82 | - 0.32 ± 0.02 | 12 | 0.913 | 0.848 | 0.4 | 12.0 | 0.857 | 4.5 | 12.8 |
| Bi | 839 | - 0.30 ± 0.02 | 12 | 1.016 | 0.896 | 0.4 | 12.0 | 0.901 | 3.6 | 12.5 |
| Mg | 12 | - 3.01 ± 0.08 | 13 | 1.094 | 1.134 | 0.3 | 13.0 | 1.110 | 23.4 | 26.8 |
| Be | 4 | - 14.04 ± 0.10 | 7 | **1.323** | 1.047 | 0.2 | 7.0 | 1.057 | 1.0 | 7.1 |
| W | 74 | - 1.34 ± 0.03 | 9 | 0.942 | 0.877 | 0.3 | 9.0 | - | - | - |
| Cu | 29 | - 1.45 ± 0.02 | 8 | 1.095 | 0.968 | 0.3 | 8.0 | 0.980 | 1.8 | 8.2 |
| Au | 79 | -1.63 ± 0.07 | 9 | 0.963 | **0.860** | **0.2** | 9.0 | - | - | - |
| Mn | 25 | - 1.53 ± 0.03 | 8 | 1.076 | 1.044 | 0.5 | 8.0 | **1.153** | 2.1 | 8.3 |
| Ta | 731 | - 2.15 ± 0.02 | 7 | 0.895 | **0.740** | **0.3** | 7.0 | **0.834** | 0.8 | 7.0 |
| V | 23 | - 1.91 ± 0.05 | 9 | 1.016 | 0.935 | 0.5 | 9.0 | 0.955 | 1.7 | 9.2 |
| Si | 14 | - 1.82 ± 0.09 | 11 | **1.207** | 0.968 | 0.3 | 11.0 | 1.013 | 4.6 | 11.9 |
| Nb | 413 | - 1.96 ± 0.04 | 8 | 0.955 | **0.851** | **0.3** | 8.0 | **0.865** | 0.8 | 8.0 |
| Co | 279 | - 1.25 ± 0.02 | 8 | **1.241** | **1.171** | **0.4** | 8.0 | **1.199** | 2.7 | 8.4 |
| U-235 | 925 | + 10.9 ± 0.07 | 7 | 0.978 | 0.925 | 0.2 | 7.0 | 0.926 | 0.3 | 7.0 |
| U-238 | 928 | - 0.703 ± 0.04 | 12 | 0.923 | 0.950 | 0.3 | 12.0 | 0.949 | 2.1 | 12.2 |
| Th | 902 | - 1.35 ± 0.04 | 9 | 0.865 | **0.833** | **0.3** | 9.0 | **0.847** | 1.5 | 9.1 |

Table 4.6. C/E values related to B-10 for SEG 7A using JEFF-3.2 and ENDF-7.1 libraries.

| Sample Material | ID No. | Exp. CRW (mc/g) | Exp. Err (%) | C/E 70g JNC JENDL -3.2 | C/E 70g JNC JEF-2.2 | C/E 33g Eur. JEF-2.2 | C/E 1968g TRIPOLI JEFF-3.2 | Calc. Err. (%) | Tot. C/E Err. (%) | C/E 1968g TRIPOLI ENDF-7.1 | Calc. Err. (%) | Tot. C/E Err. (%) |
|---|---|---|---|---|---|---|---|---|---|---|---|---|
| B-10 | 105 | - 850 ± 10 | 2 | 1.000 | 1.000 | 1.000 | 1.000 | 0.3 | 2.0 | 1.000 | 0.4 | 2.0 |
| C | 6 | - 1.9 ± 0.05 | 6 | 1.035 | 1.041 | 1.091 | **1.119** | **0.4** | 6.0 | **1.128** | **0.6** | 6.0 |
| U-235 | 925 | + 28.0 ± 3.0 | 13 | 1.149 | 1.144 | 1.150 | 1.142 | 0.4 | 13.0 | 1.137 | 0.5 | 13.0 |
| Ta | 731 | - 26.0 ± 1.0 | 7 | **0.868** | **0.867** | 0.928 | 0.899 | 0.9 | 7.1 | 0.935 | 1.2 | 7.1 |
| Cd | 48 | | 15 | | | **1.304** | - | - | - | - | - | - |
| Mo-95 | 425 | - 16.8 ± 2.5 | **18** | 0.940 | 1.050 | 0.960 | 1.006 | 2.7 | 18.2 | 0.968 | 2.9 | 18.2 |
| Mo-97 | 427 | - 8.0 ± 0.6 | 11 | 0.956 | 0.982 | 0.961 | 0.993 | 0.9 | 11.0 | 1.010 | 1.1 | 11.1 |
| Mo-98 | 428 | - 2.7 ± 1.0 | **40** | 1.133 | 1.164 | 1.141 | 1.222 | 1.7 | 40.0 | 1.192 | 1.9 | 40.0 |
| Mo-100 | 420 | - 8.1 ± 1.0 | 13 | **0.300** | **0.286** | **0.471** | **0.306** | **1.7** | 13.1 | **0.281** | **1.8** | 13.1 |

| | | | | | | | | | | | | |
|---|---|---|---|---|---|---|---|---|---|---|---|---|
| Rh-103 | 453 | - 15.0 ± 2.0 | 16 | 1.168 | **1.230** | 1.118 | 1.141 | 1.2 | 16.0 | 1.092 | 1.3 | 16.1 |
| Ag-109 | 479 | - 36.0 ± 1.5 | 7 | **0.820** | 0.901 | 0.894 | **0.853** | **1.9** | 7.2 | **0.838** | **2.3** | 7.4 |
| Sm-149 | 629 | - 70.0 ± 3.0 | 7 | **1.751** | **1.337** | **1.498** | **1.357** | **1.6** | 7.2 | **1.299** | **1.8** | 7.2 |

Table 4.7. Reactivity contributions for SEG 5 using JEF-3.2.

| Sample Material | Scat/Tot (%) JNC 70=>18g JENDL-3.2 | Scat/Tot (%) JNC 70=>18g JEF-2.2 | Scat/Tot (%) JNC 70g JENDL-3.2 | Scat/Tot (%) European 1968=>33g JEF-2.2 | Elas./Tot (%) TRIPOLI 1968g JEF-3.2 | Calc. Error (%) | Inel./Tot (%) TRIPOLI 1968g JEF-3.2 | Calc. Error (%) | Scat/Tot (%) TRIPOLI 1968g JEF-3.2 |
|---|---|---|---|---|---|---|---|---|---|
| B-10 ss | +0.10 | +0.08 | +0.01 | -0.012 | -0.025 | 2.6 | -0.025 | 2.6 | -0.050 |
| Ta | +0.45 | | +0.26 | -0.02 | -0.347 | 21.5 | -0.347 | 21.5 | -0.694 |
| U-235 | -0.17 | -0.19 | -0.12 | +0.008 | 0.011 | 33.6 | 0.157 | 0.4 | 0.168 |
| Mo | +2.5 | +2.9 | +1.5 | +0.12 | 1.089 | 23.6 | 1.089 | 2.2 | 2.178 |
| Mn | +9.3 | +4.5 | +3.9 | +0.12 | 4.912 | 22.0 | -0.554 | 1.4 | 4.358 |
| Cd | +1.2 | | +0.76 | -0.14 | -1.080 | 9.7 | -0.983 | 2.4 | -2.062 |
| Nb | +1.6 | | +0.97 | -0.05 | 0.059 | 59.3 | -0.897 | 0.8 | -0.837 |
| Cu | +5.4 | +4.8 | +1.5 | -0.61 | -7.395 | 5.1 | -1.478 | 1.9 | -8.873 |
| Zr | +7.5 | +9.1 | +4.8 | -0.27 | -0.862 | 62.0 | -3.385 | 2.1 | -4.247 |
| W | +3.8 | | +1.2 | +0.10 | 2.310 | 34.3 | -0.658 | 2.8 | 1.652 |
| Fe | +19.6 | +20.8 | +9.7 | -8.0 | 3.157 | 30.1 | -7.636 | 3.2 | -4.479 |
| Cr | +12.8 | +14.4 | +2.7 | -12.3 | -5.237 | 18.5 | -5.964 | 2.6 | -11.202 |
| Ni | +11.2 | +11.9 | -4.5 | -11.1 | 0.741 | 102.2 | -1.621 | 5.8 | -0.879 |
| Co | +1.5 | | +2.9 | +0.21 | 3.043 | 43.4 | -0.271 | 2.6 | 2.773 |
| Mo-95 | +1.1 | | +0.75 | +0.64 | 0.957 | 27.2 | -0.624 | 2.9 | 0.333 |
| Mo-97 | +1.3 | | +0.77 | -0.12 | 0.058 | 44.6 | -1.114 | 0.8 | -1.056 |
| Mo-98 | +6.3 | | +2.5 | +0.01 | -2.954 | 6.8 | -1.851 | 1.7 | -4.804 |
| Mo-100 | +3.4 | | +2.9 | -0.12 | 5.606 | 9.8 | -2.635 | 2.2 | 2.971 |
| Rh-103 | +0.6 | | +0.38 | -0.07 | -0.161 | 14.6 | -0.460 | 0.8 | -0.622 |
| Pd-105 | +0.4 | | +0.28 | -0.07 | 0.081 | 10.9 | -0.438 | 0.5 | -0.357 |
| Ag-109 | +0.5 | | +0.31 | -0.03 | 0.020 | 133.0 | -0.361 | 1.2 | -0.341 |
| Cs-133 | +0.6 | | +0.43 | -0.03 | 0.505 | 16.0 | -0.284 | 1.2 | 0.221 |
| Nd-143 | +1.0 | | +0.55 | +0.99 | -0.204 | 161.8 | -0.240 | 1.3 | -0.444 |
| Nd-145 | +2.0 | | +0.44 | +0.81 | -1.544 | 15.9 | -0.387 | 1.0 | -1.932 |
| Sm-149 | +0.2 | | +0.09 | +0.02 | 0.055 | 54.4 | -0.090 | 1.9 | -0.035 |
| Eu-153 | +0.2 | | +0.10 | -0.01 | -0.037 | 15.3 | -0.101 | 0.5 | -0.138 |

Table 4.8. Reactivity contributions for SEG 7A using JEF-3.2.

| Sample Material | ID-No. | Elas./Tot (%) TRIPOLI 1968g JEF-3.2 | Calc. Error (%) | Inel./Tot (%) TRIPOLI 1968g JEF-3.2 | Calc. Error (%) | Scat/Tot (%) TRIPOLI 1968g JEF-3.2 |
|---|---|---|---|---|---|---|
| B-10 | 105 | 0.231 | 0.4 | 0.004 | 0.6 | 0.23 |
| C | 6 | 98.729 | 0.5 | 0.325 | 1.8 | 99.05 |
| U-235 | 925 | -0.025 | 8.4 | -0.464 | 0.4 | -0.49 |
| Ta | 731 | 0.194 | 20.8 | 0.827 | 1.0 | 1.02 |

| | | | | | | |
|---|---|---|---|---|---|---|
| Cd | 48 | - | - | - | - | - |
| Mo-95 | 425 | 3.814 | 5.7 | 1.614 | 2.7 | 5.43 |
| Mo-97 | 427 | 0.855 | 3.8 | 4.389 | 0.9 | 5.24 |
| Mo-98 | 428 | 6.037 | 5.1 | 6.976 | 1.7 | 13.01 |
| Mo-100 | 420 | 3.442 | 6.5 | 10.258 | 1.7 | 13.70 |
| Rh-103 | 453 | 0.102 | 15.6 | 1.600 | 1.2 | 1.70 |
| Ag-109 | 479 | 0.424 | 6.9 | 0.859 | 1.9 | 1.28 |
| Sm-149 | 629 | -0.021 | 111.5 | 0.258 | 1.6 | 0.24 |

Table 4.9. Reactivity contributions for SEG 6 EK_45 using JEF-3.2.

| | JNC route with JENDL-3.2 | | | | ECCO/ERANOS/JEF-2.2 | | | | TRIPOLI4 with JEFF-3.2 (1968g) | | | |
|---|---|---|---|---|---|---|---|---|---|---|---|---|
| Sample Material | Capture (%) | El. Scat. (%) | Inel. Scat. (%) | Fis. (%) | Capture (%) | El. Scat. (%) | Inel. Scat. (%) | Fis. (%) | Capture (%) | El. Scat. (%) | Inel. Scat. (%) | Fis. (%) |
| H | 0.004 | 100.0 | 0.0 | | 0. | 100 | 0. | | 0.00 | 100.0 | 0.00 | |
| C | 0.46 | 98.4 | 1.2 | | 0.4 | 98.6 | 1.0 | | 0.3 | 98.7 | 1.0 | |
| B-10 | 89.6 | 9.8 | 0.6 | | 90.4 | 9.4 | 0.2 | | 88.0 | 11.8 | 0.2 | |
| Mo | 25.6 | 11.5 | 62.7 | | 23.2 | 12.8 | 64.0 | | 23.1 | 14.8 | 11.1 | |
| Fe | 9.0 | 25.5 | 65.5 | | 6.1 | 25.9 | 68.0 | | 7.0 | 32.9 | 60.1 | |
| Cr | 6.5 | 35.5 | 58.1 | | 5.7 | 33.2 | 61.1 | | 4.1 | 38.3 | 57.6 | |
| Ni | 32.7 | 37.7 | 30.1 | | 35.9 | 39.6 | 24.5 | | 30.1 | 36.8 | 33.1 | |
| Al | 3.5 | 68.6 | 28.0 | | 3.8 | 68.0 | 28.2 | | 2.8 | 66.8 | 30.5 | |
| Zr | 10.0 | 23.9 | 66.0 | | 7.6 | 28.5 | 63.9 | | 8.5 | 30.9 | 60.6 | |
| Ti | 6.5 | 45.3 | 48.2 | | 6.3 | 51.4 | 42.3 | | | | | |
| Cd | 39.5 | 6.9 | 53.3 | | 32.8 | 7.6 | 59.6 | | 32.3 | 6.5 | 61.1 | |
| Pb | 2.7 | 11.8 | 84.2 | | 3.8 | 20.2 | 76.0 | | 3.1 | 16.6 | 79.9 | |
| Bi | 4.2 | 14.7 | 79.7 | | 4.6 | 20.1 | 75.3 | | 2.6 | 18.6 | 78.3 | |
| Mg | 3.4 | 73.3 | 23.4 | | 2.3 | 76.7 | 21.0 | | 2.9 | 76.6 | 20.5 | |
| Be | 6.4 | 79.9 | 13.7 | | 6.1 | 82.1 | 11.8 | | 6.2 | 97.5 | 0.0 | |
| W | 24.8 | 3.6 | 70.7 | | 26.7 | 5.2 | 68.1 | | 23.9 | 4.4 | 71.5 | |
| Cu | 18.6 | 21.7 | 59.8 | | 18.2 | 26.6 | 55.2 | | 16.3 | 26.6 | 57.1 | |
| Au | | | | | 43.3 | 3.7 | 53.0 | | 39.5 | 3.5 | 56.9 | |
| Mn | 6.8 | 32.2 | 61.0 | | 8.9 | 30.5 | 60.6 | | 5.3 | 27.1 | 67.6 | |
| Ta | 50.0 | 2.3 | 47.4 | | 49.7 | 2.8 | 47.5 | | 42.5 | 3.2 | 54.2 | |
| V | 5.0 | 45.7 | 49.4 | | 3.4 | 43.5 | 53.1 | | 3.8 | 49.4 | 46.8 | |
| Si | 6.1 | 68.4 | 25.7 | | 6.0 | 74.0 | 20.0 | | 5.3 | 72.2 | 22.4 | |
| Nb | 28.3 | 12.1 | 59.6 | | 28.4 | 57.7 | 13.9 | | 27.3 | 13.1 | 59.5 | |
| Co | 9.5 | 28.9 | 61.7 | | 8.1 | 31.5 | 60.4 | | 7.5 | 31.6 | 60.8 | |
| U-235 | 6.8 | 0.3 | 6.0 | 113.2 | 6.5 | 0.3 | 6.1 | 112.9 | -5.4 | -0.3 | -7.1 | 112.8 |
| U-238 | 57.7 | 5.4 | 115.7 | 81.0 | 62.8 | 5.0 | 113.8 | 81.6 | 48.4 | 7.0 | 109.2 | -65.0 |
| Th-232 | 38.6 | 3.1 | 65.5 | 8.7 | 48.5 | 2.7 | 56.6 | 7.8 | 38.9 | 3.3 | 64.5 | -7.0 |

## 4.4 SENSITIVITIES

The cross-section sensitivities have been broken down into capture, elastic scatter, inelastic scatter, and fission for some of the more important isotopes measured in the RRR/SEG experiments. These are given for JEF-3.2 and ENDF-7.1 in a 33 group structure. For U-235 the competing effects are clearly between capture and fission in SEG 4, 5, 7A, and 7B, with the fission contribution dominant. In SEG 6EK_45 the inelastic contribution at high energies can be observed, and for U-238 it is the dominant effect. The softer spectrums in SEG 7A and 7B clearly shift the sensitivities to lower energies. The capture effect dominates that due to fission for U-238 making the net reactivity effect positive. The Fe-56 sensitivities in SEG 5 and 6 compare very well to previous analyses [19, 18].

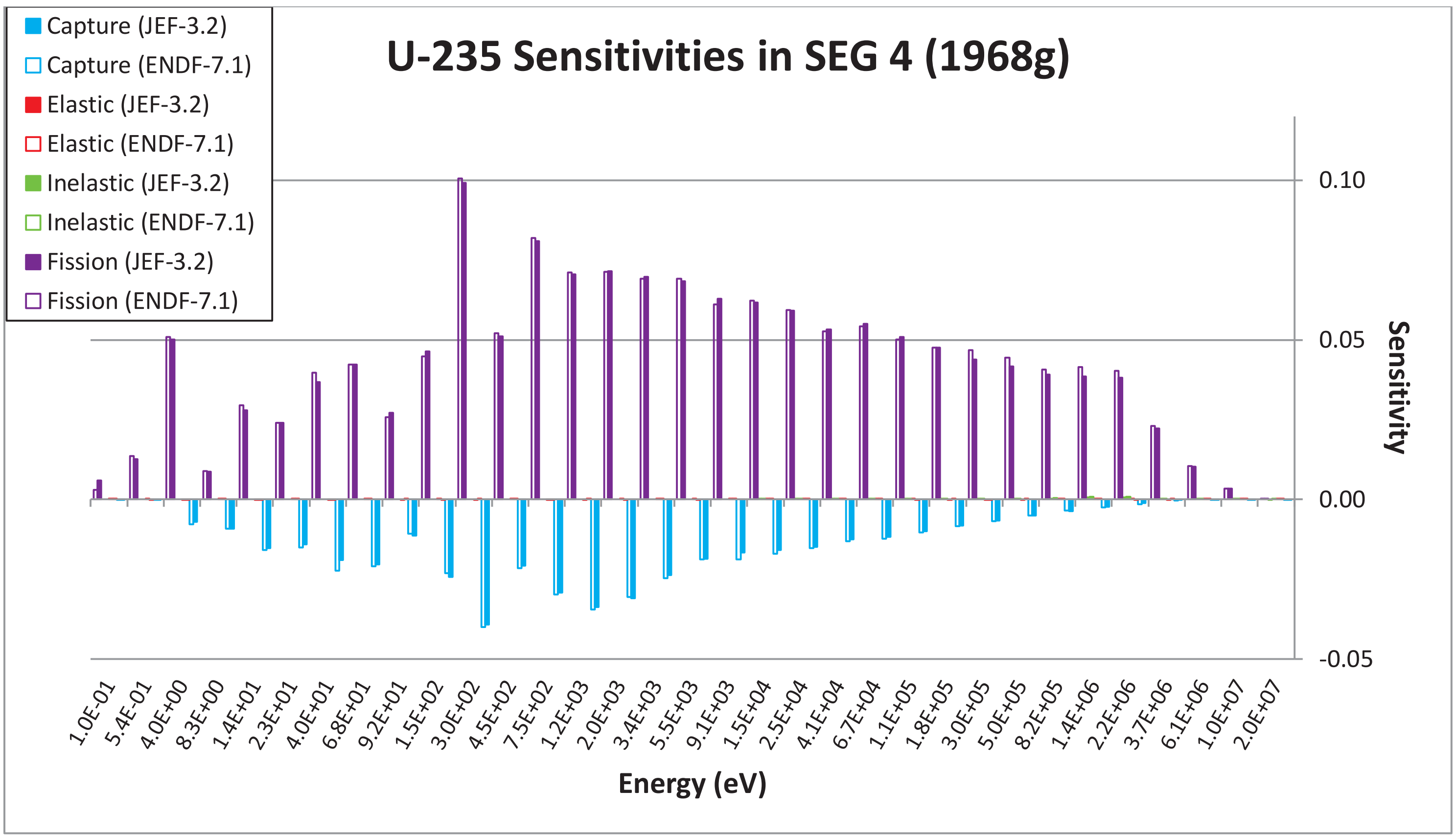


Figure 4.16 U-235 sensitivities in SEG 4.

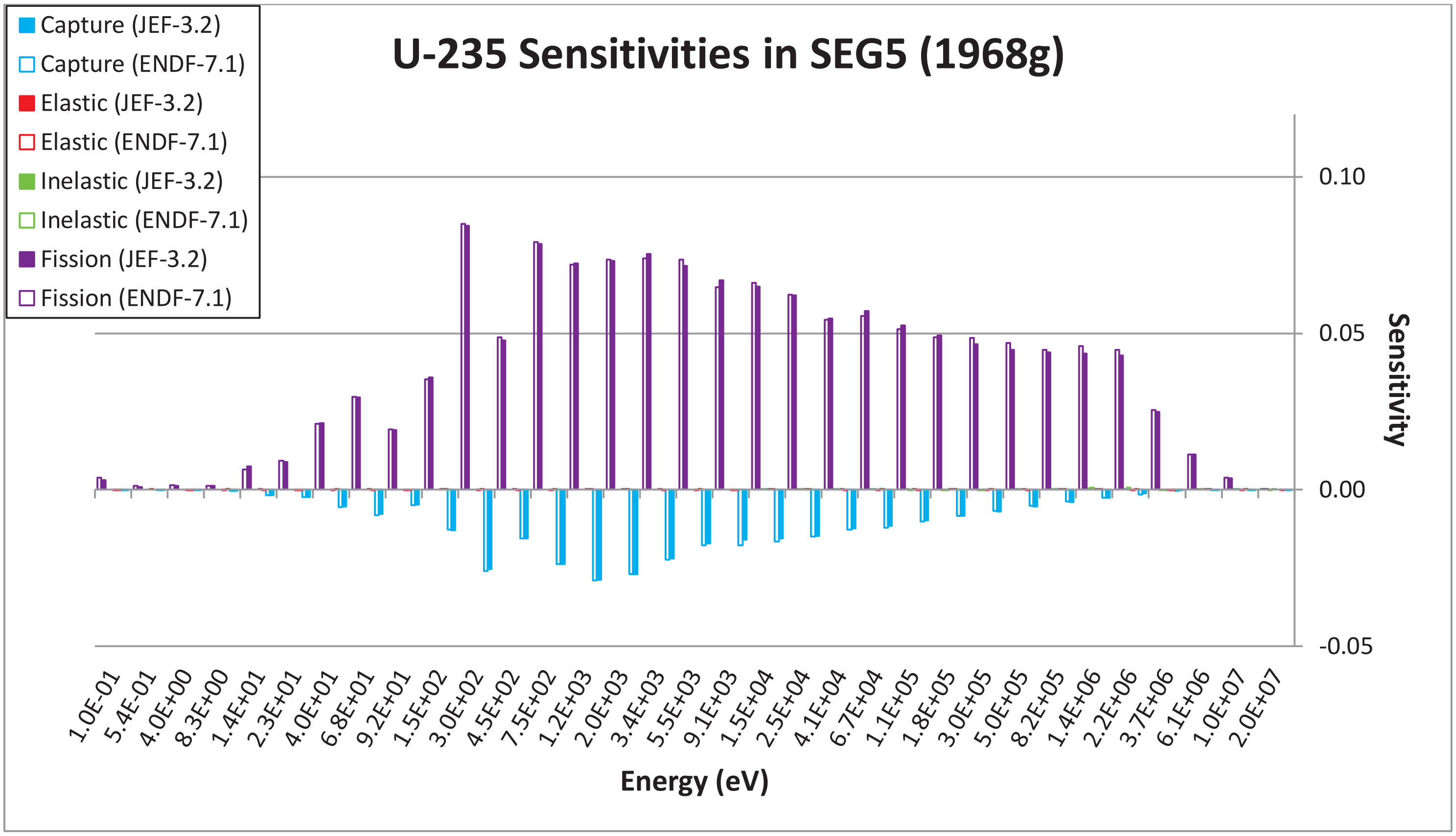


Figure 4.17 U-235 Sensitivities in SEG 5.

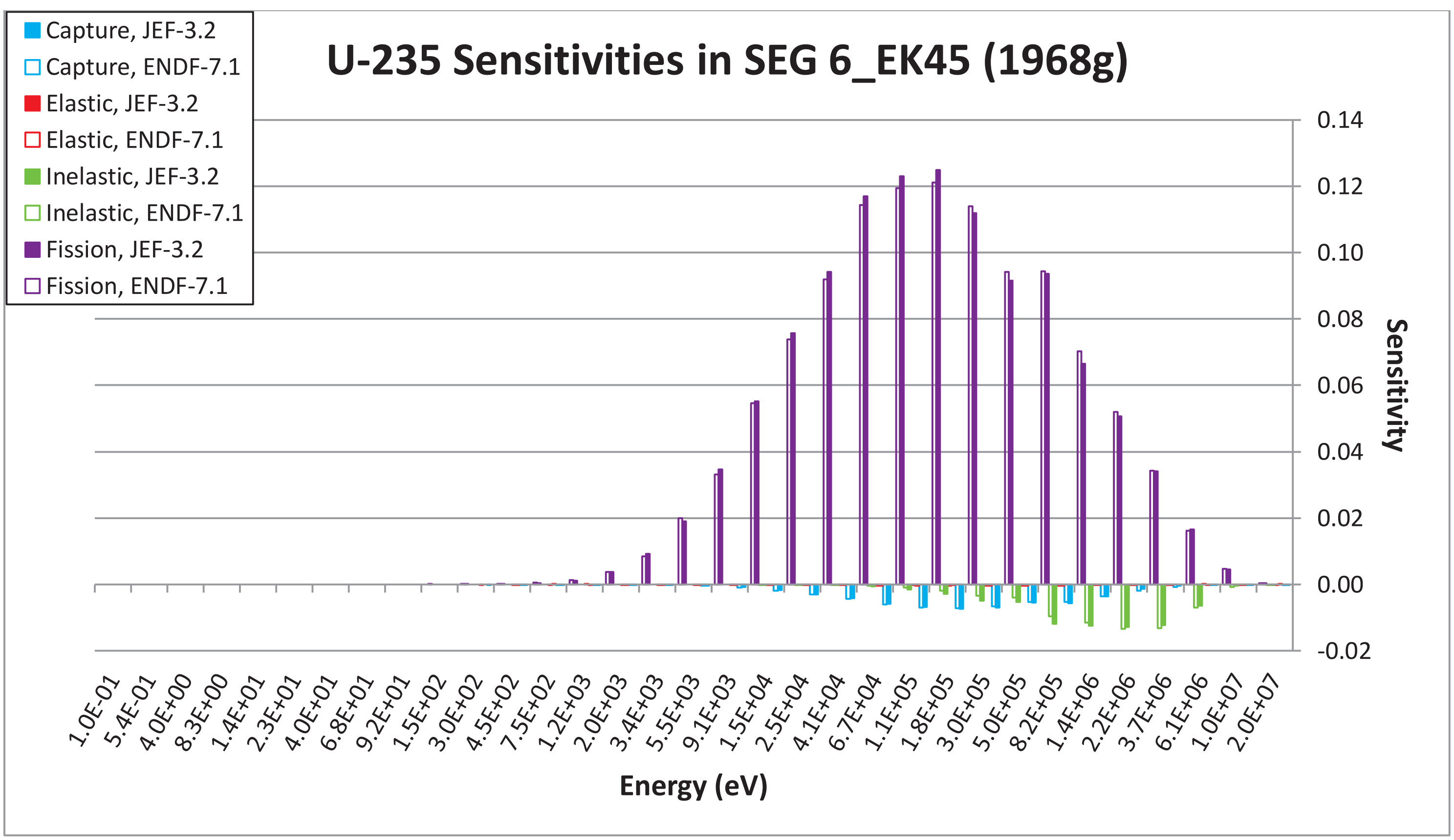


Figure 4.18 U-235 sensitivities in SEG 6 EK_45.

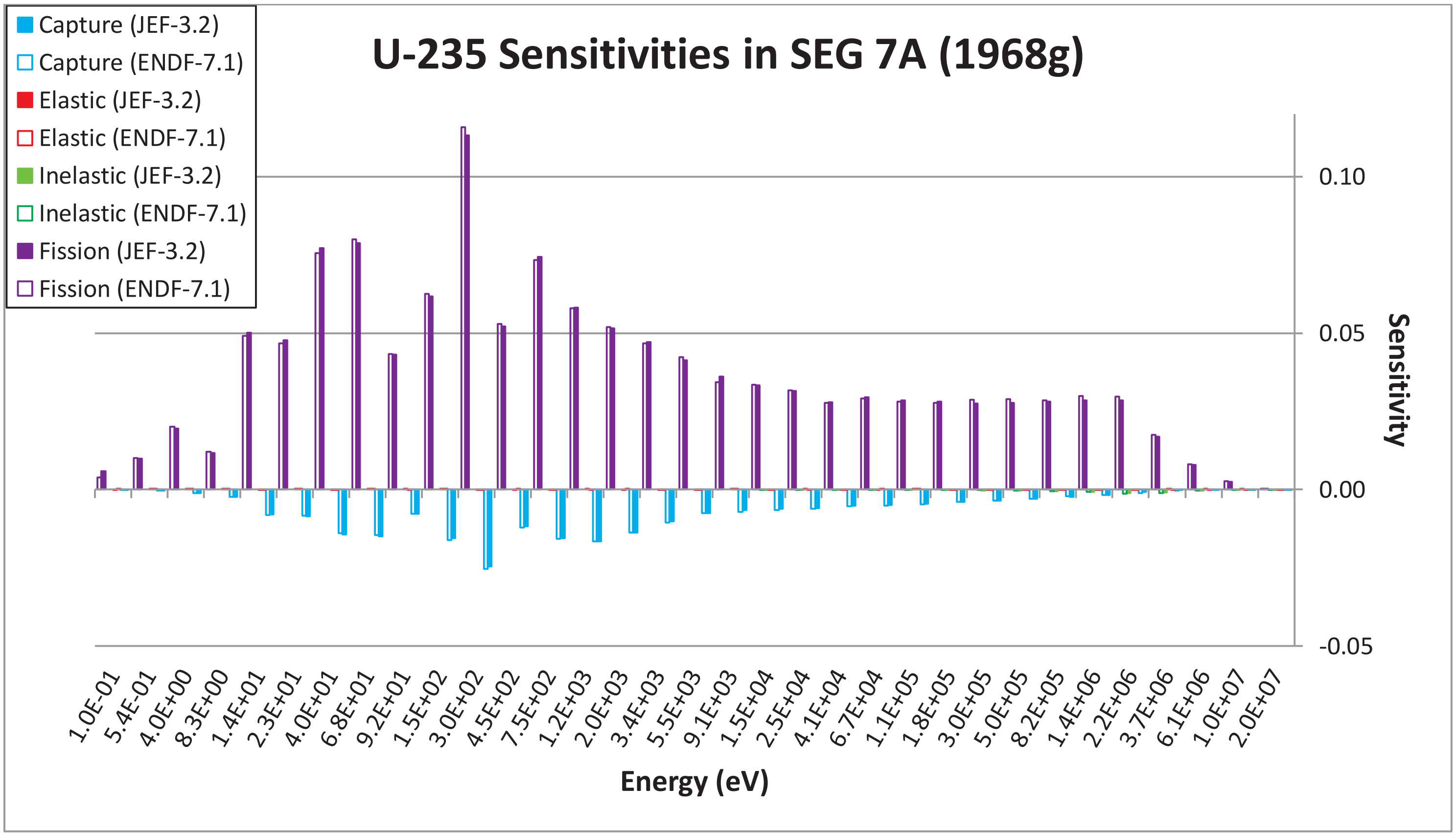


Figure 4.19 U-235 Sensitivities in SEG 7A.

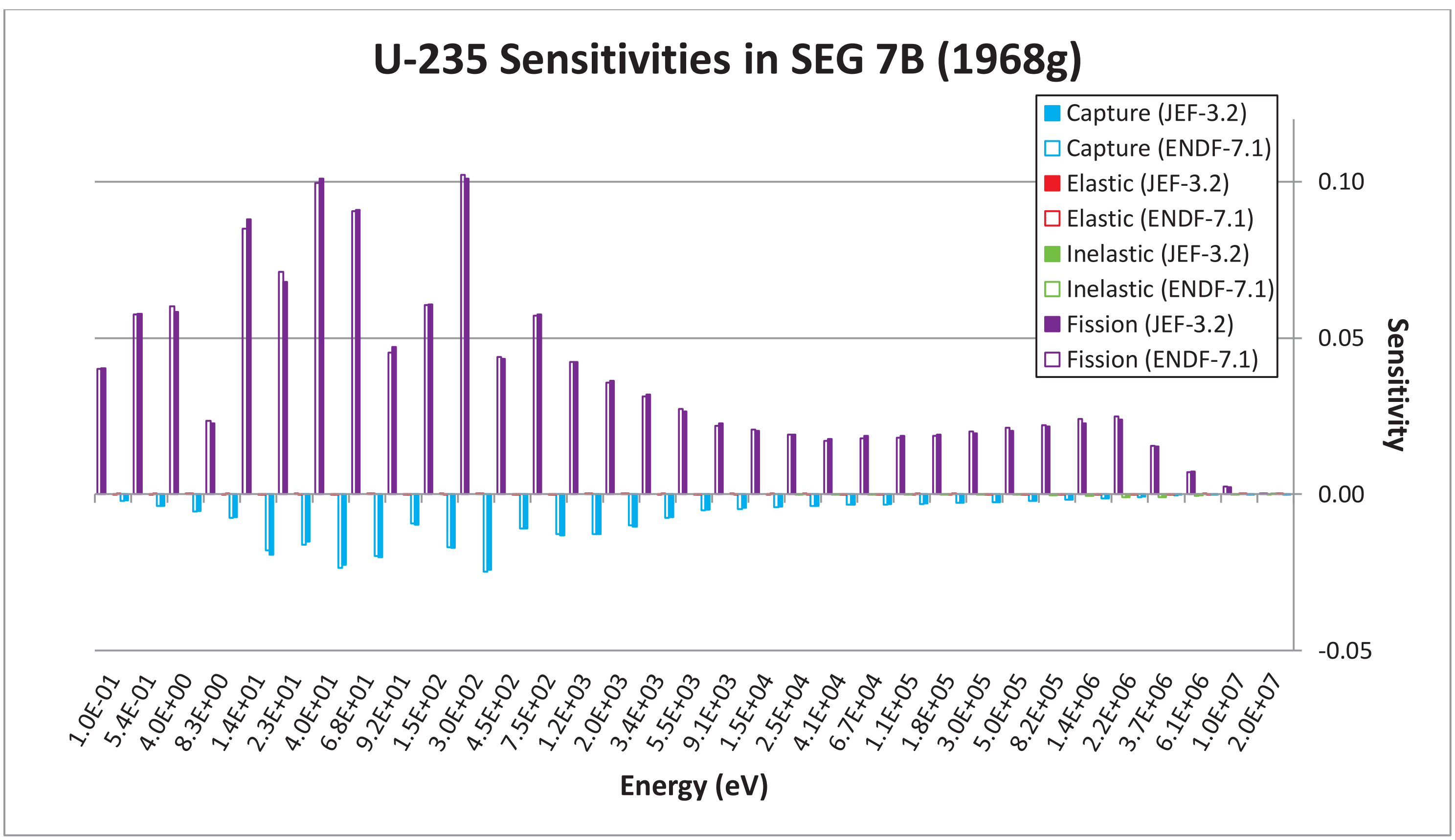


Figure 4.20 U-235 sensitivities in SEG 7B.

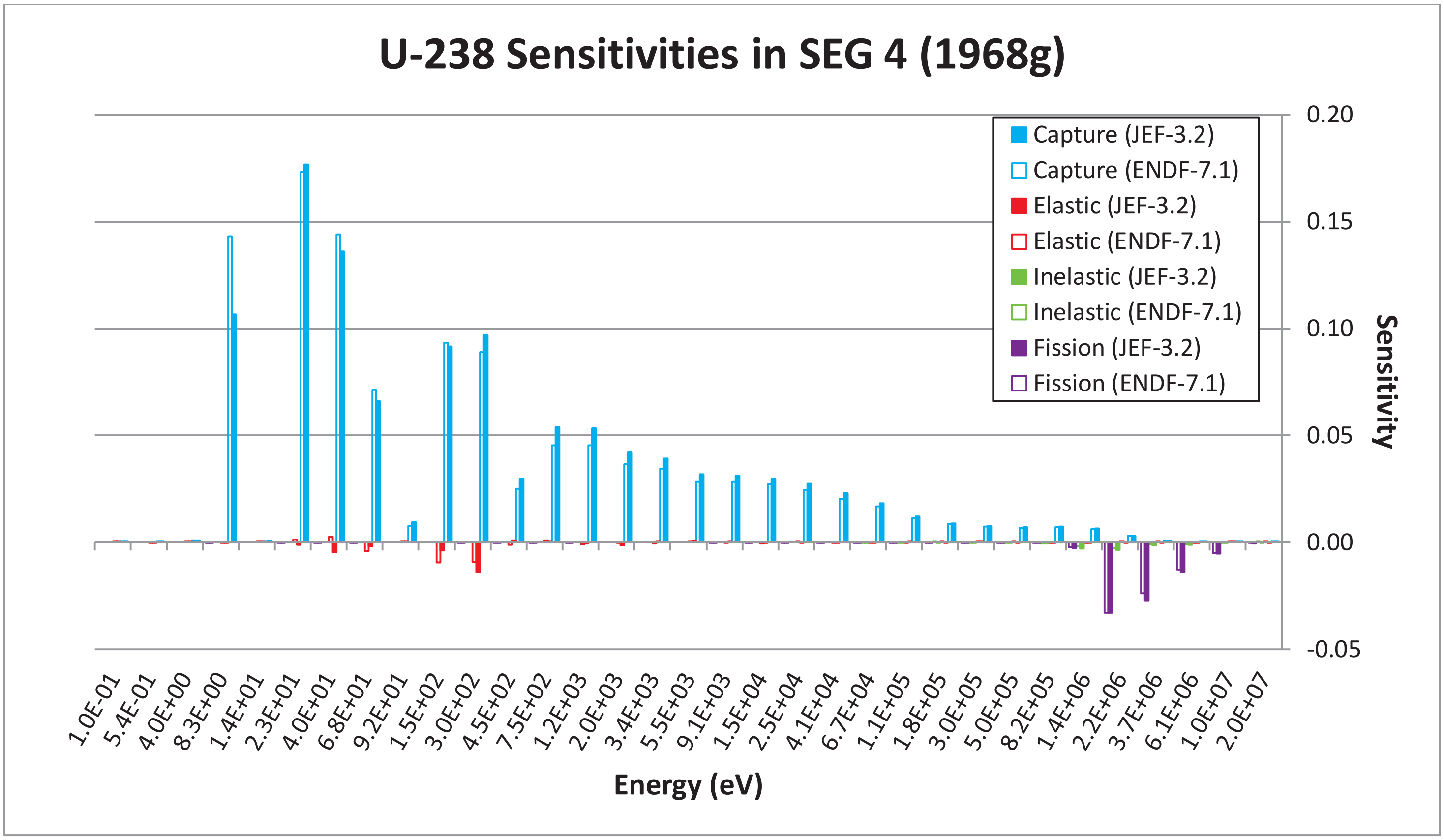


Figure 4.21 U-238 sensitivities in SEG 4.

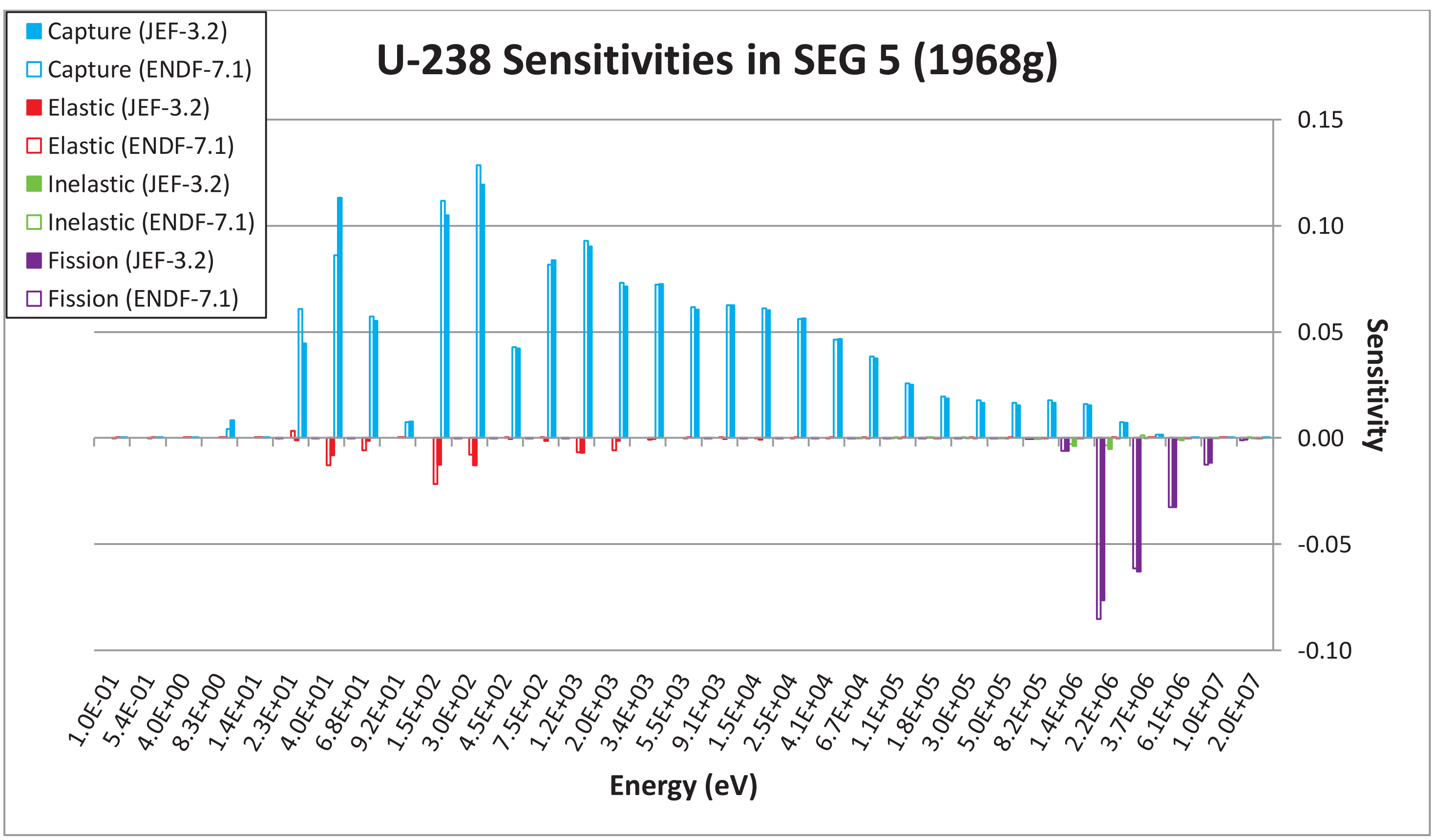


Figure 4.22 U-238 sensitivities in SEG 5.

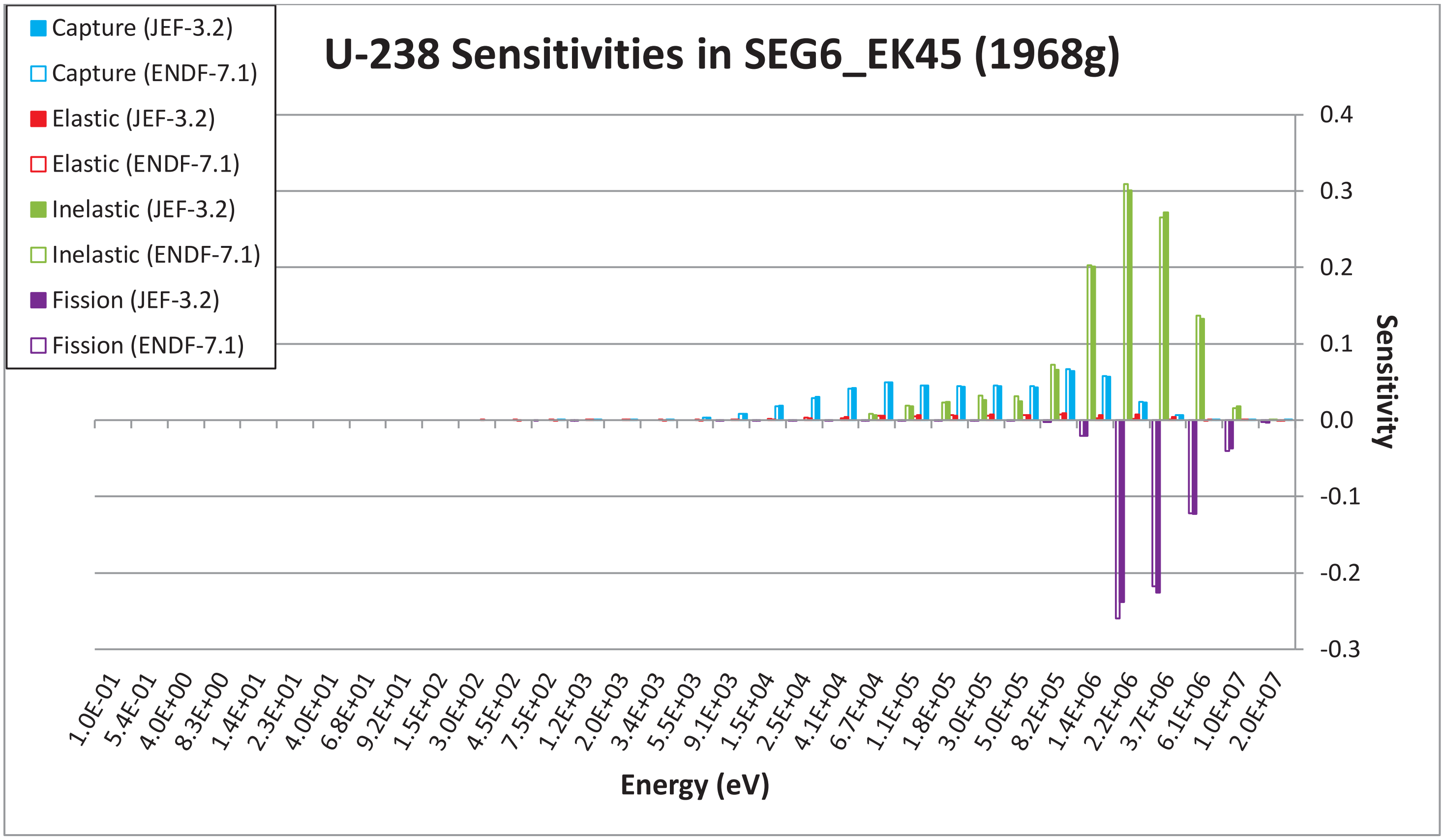


Figure 4.23 U-238 sensitivities in SEG 6 EK_45.

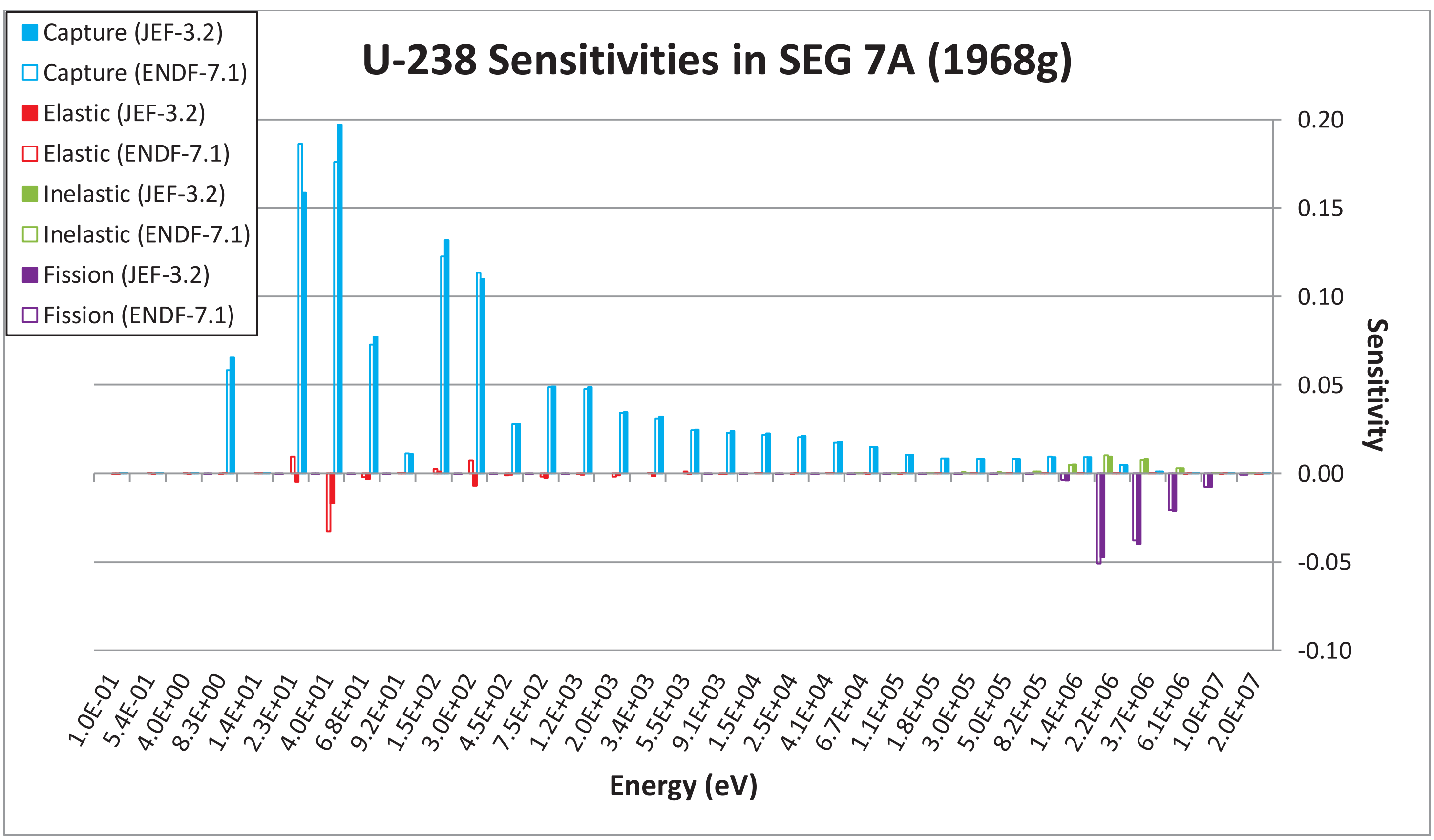


Figure 4.24 U-238 sensitivities in SEG 7A.

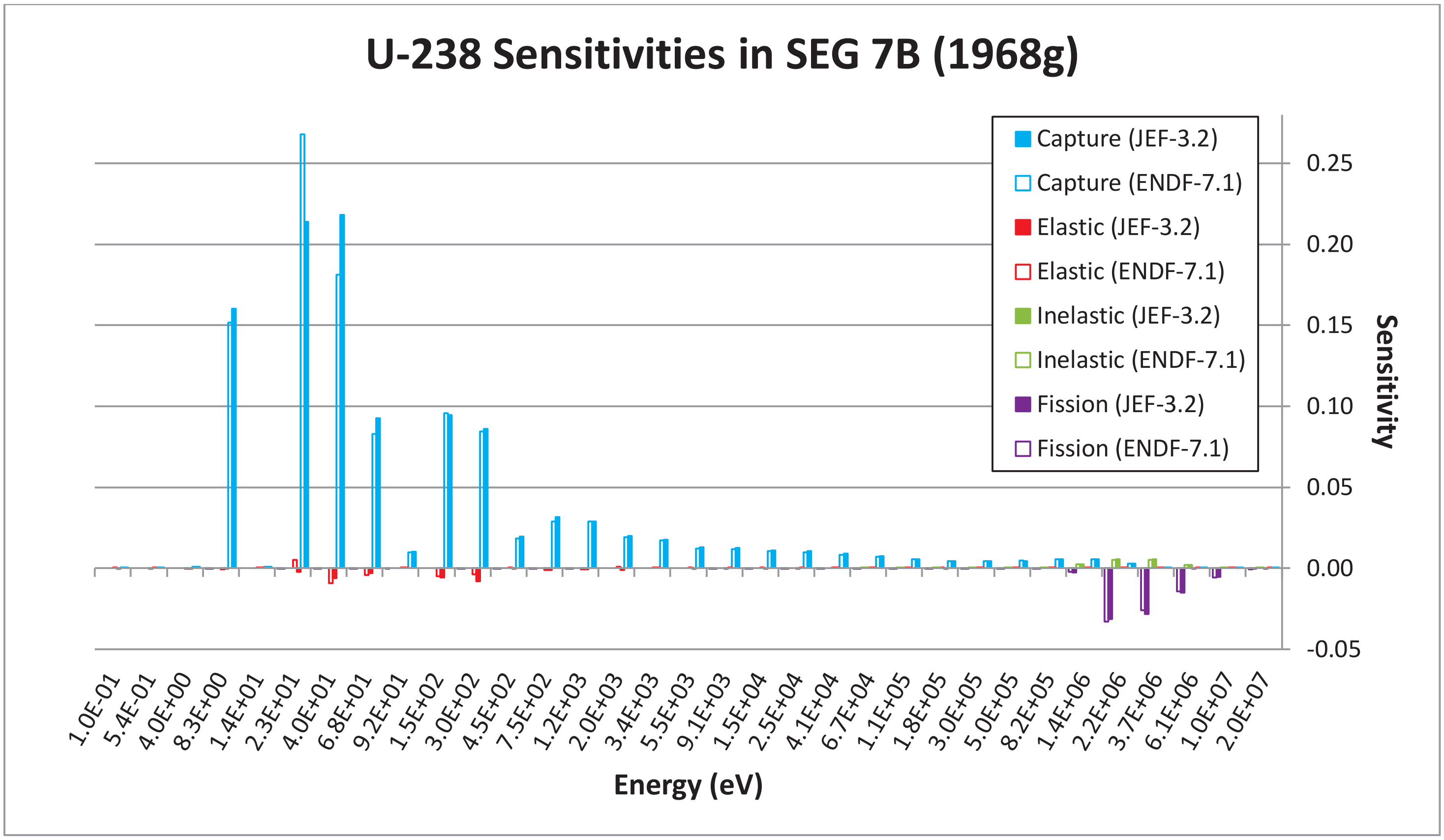


Figure 4.25 U-238 sensitivities in SEG 7B.

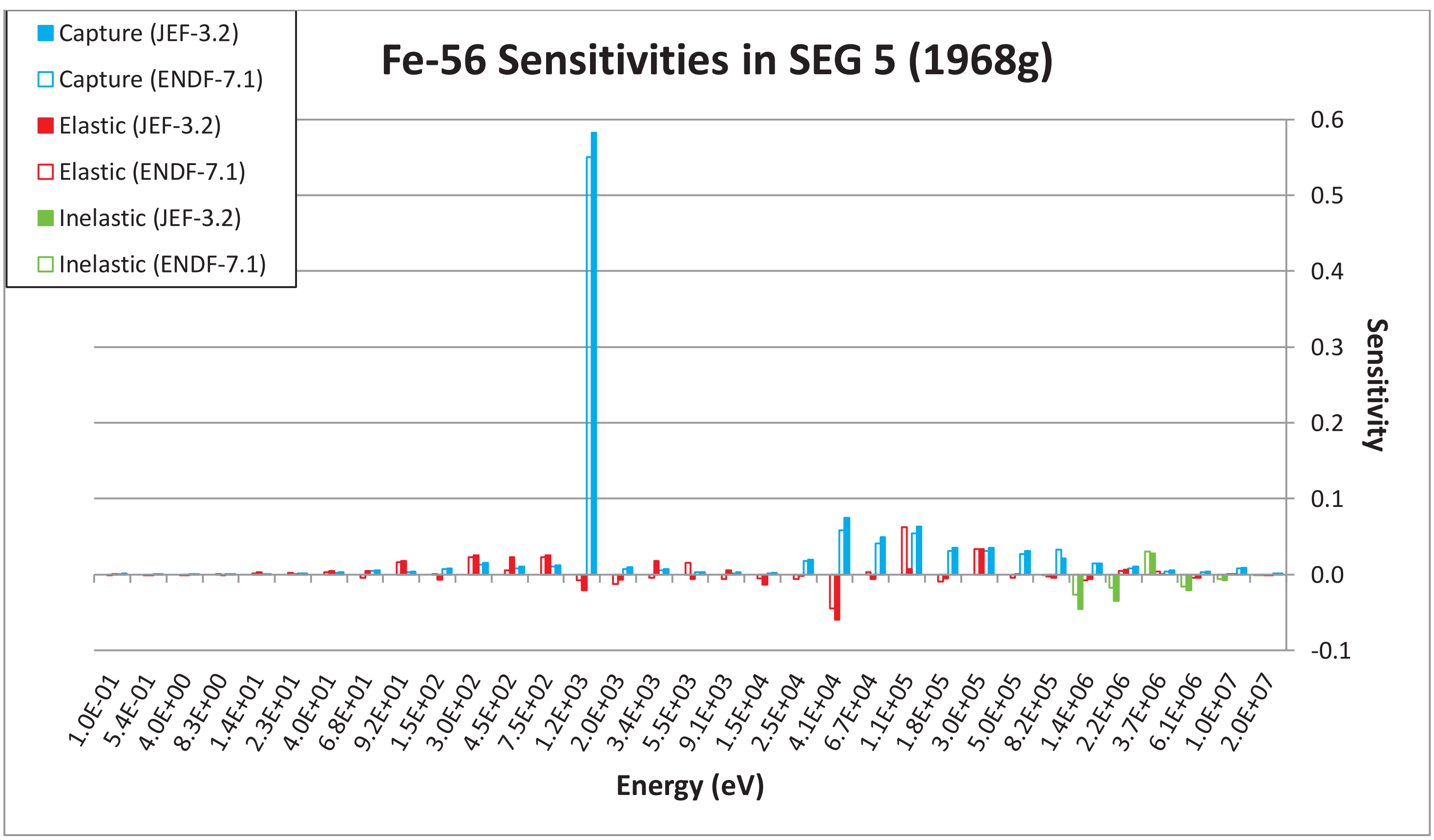


Figure 4.26 Fe-56 sensitivities in SEG 5.

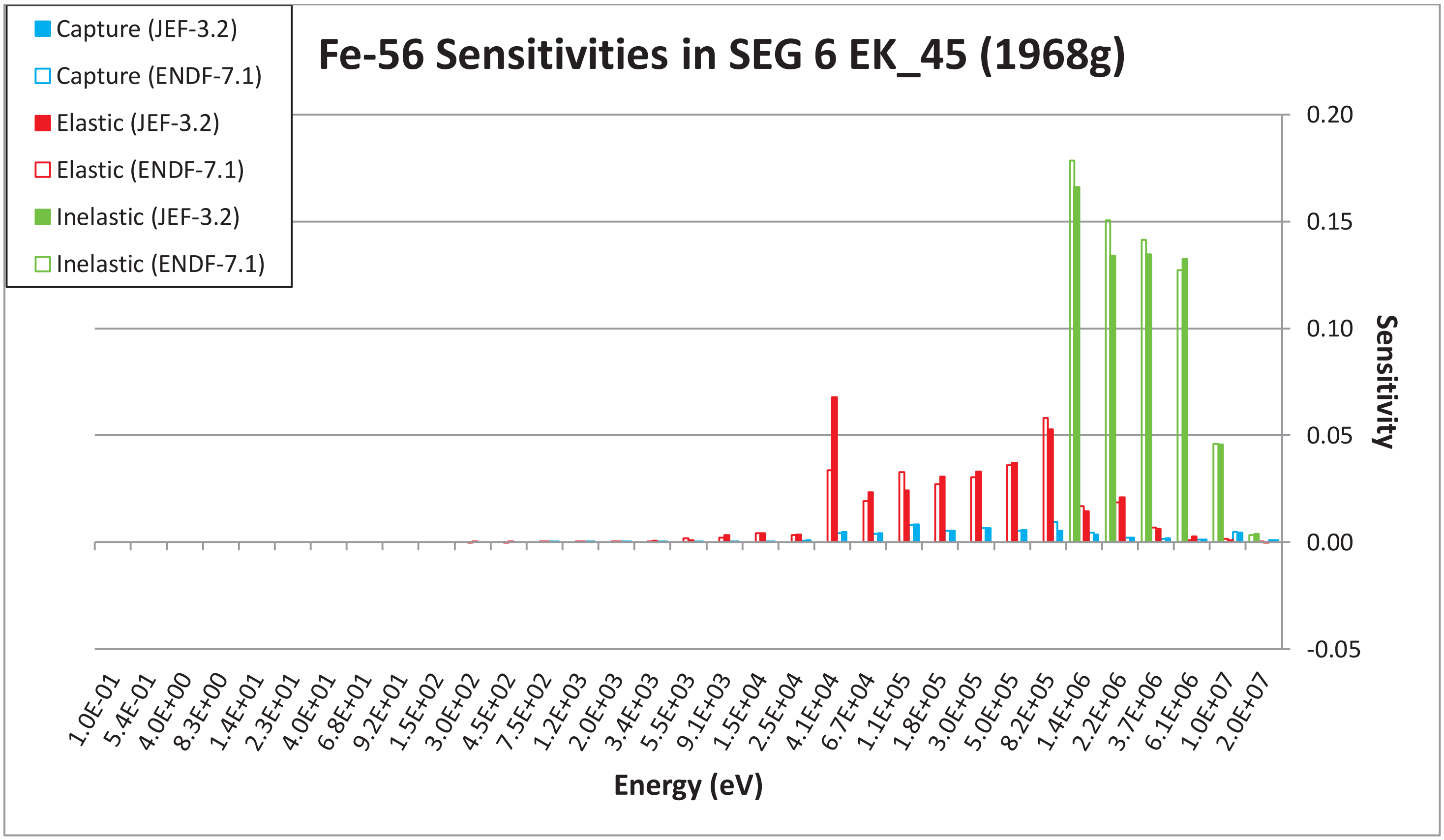

Figure 4.27 Fe-56 sensitivities in SEG 6 EK_45.

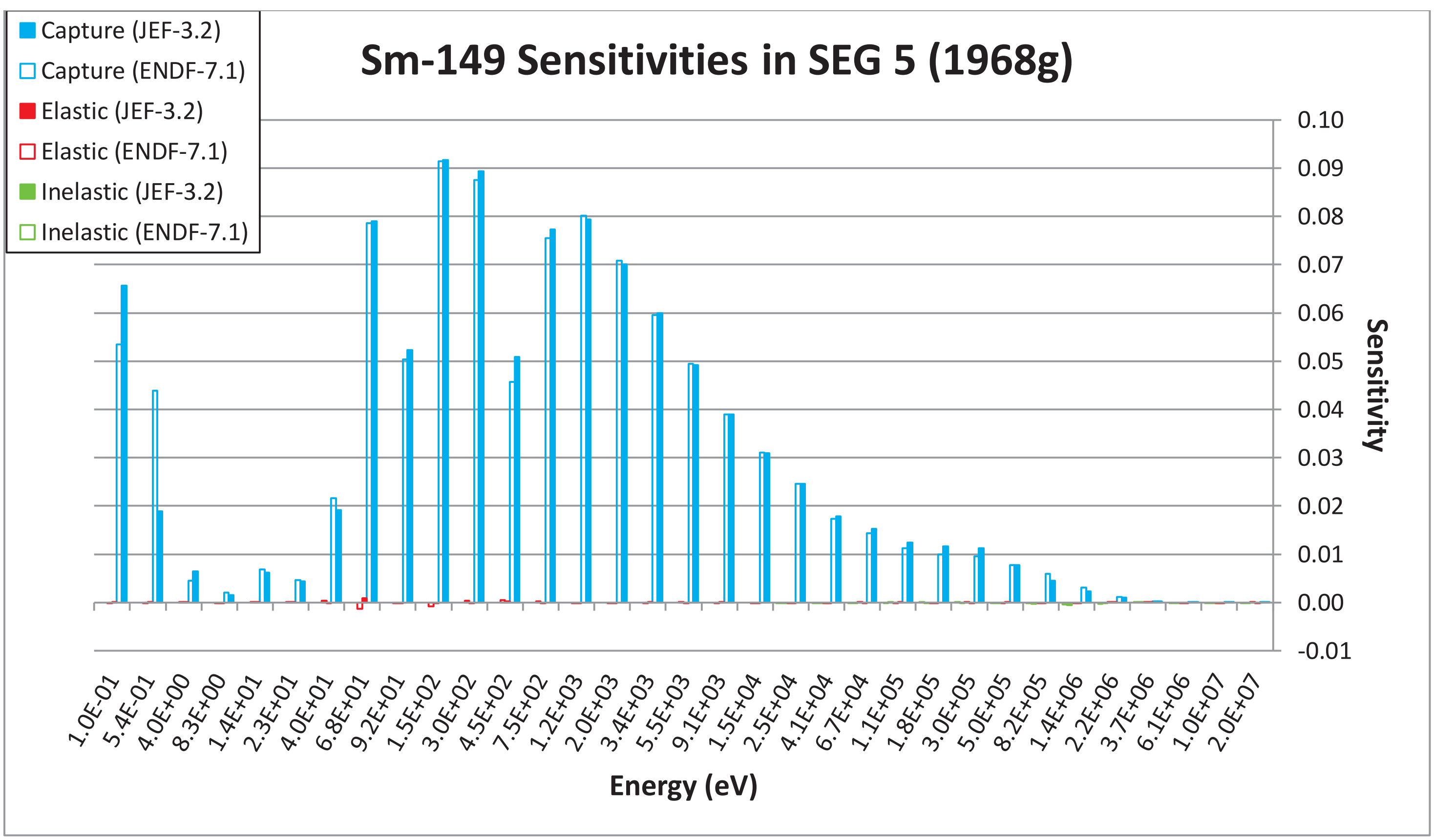

Figure 4.28 Sm-149 sensitivities in SEG 5.

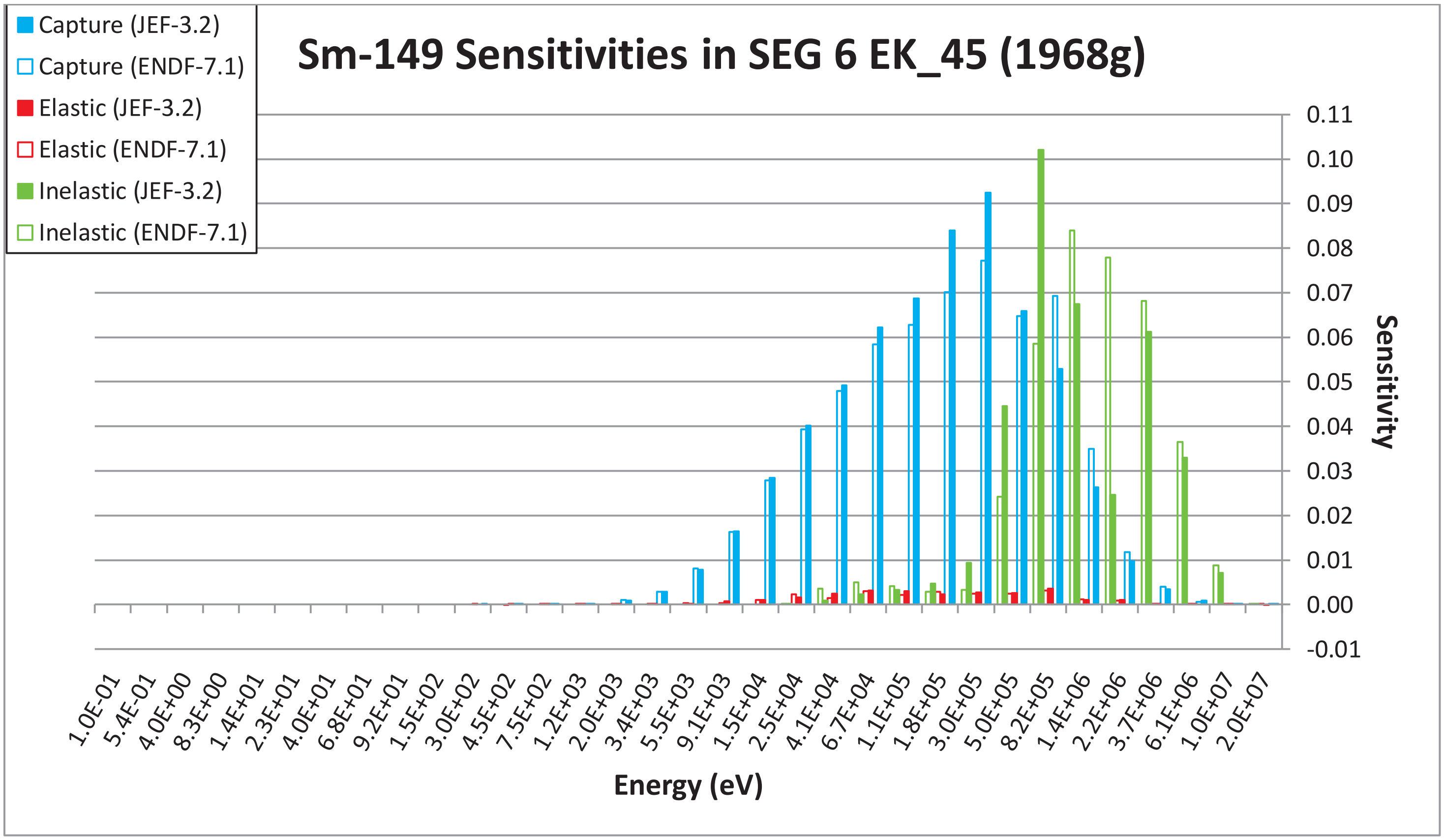


Figure 4.29 Sm-149 sensitivities in SEG 6 EK_45.

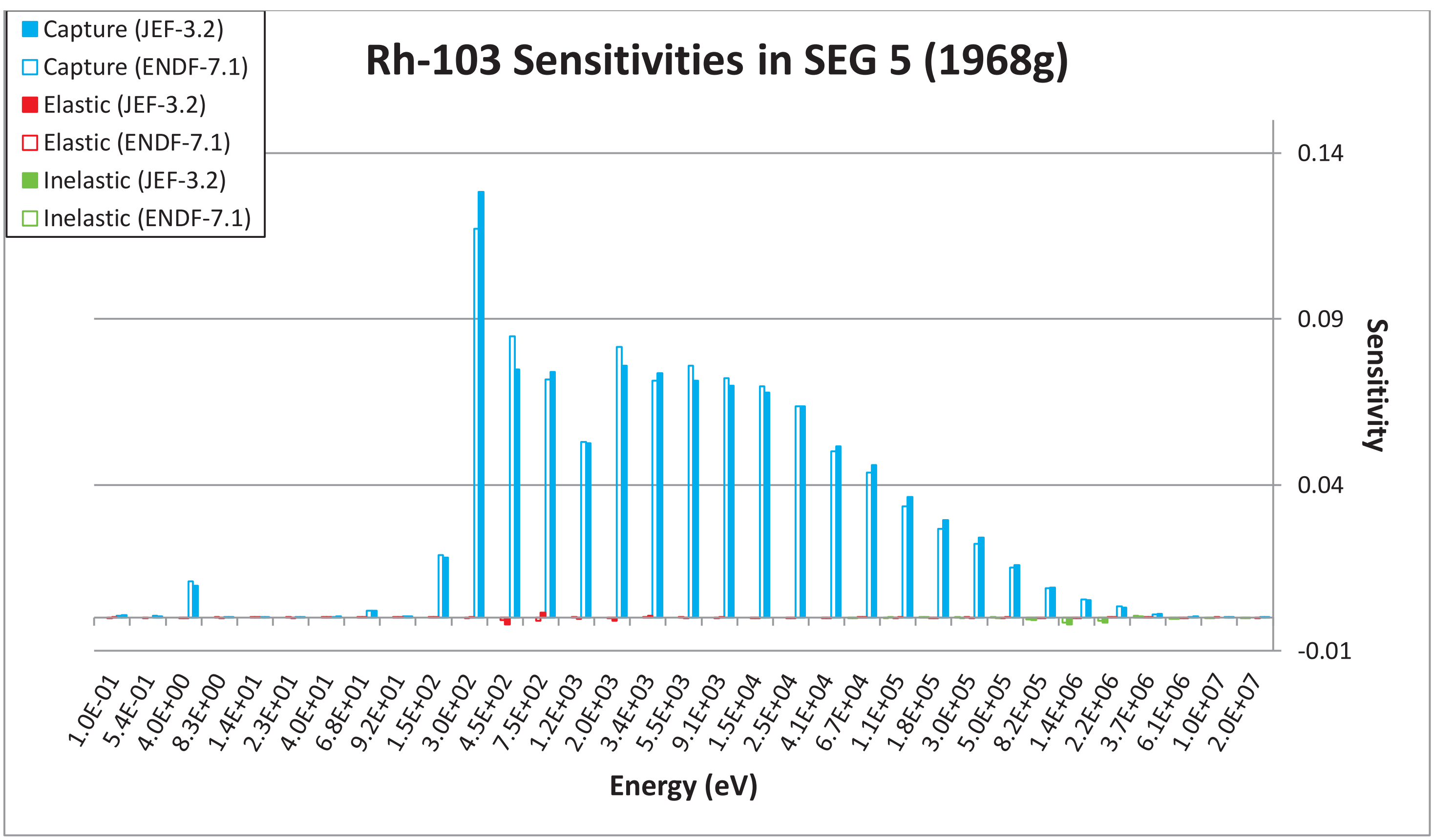


Figure 4.30 Rh-103 sensitivities in SEG 5.

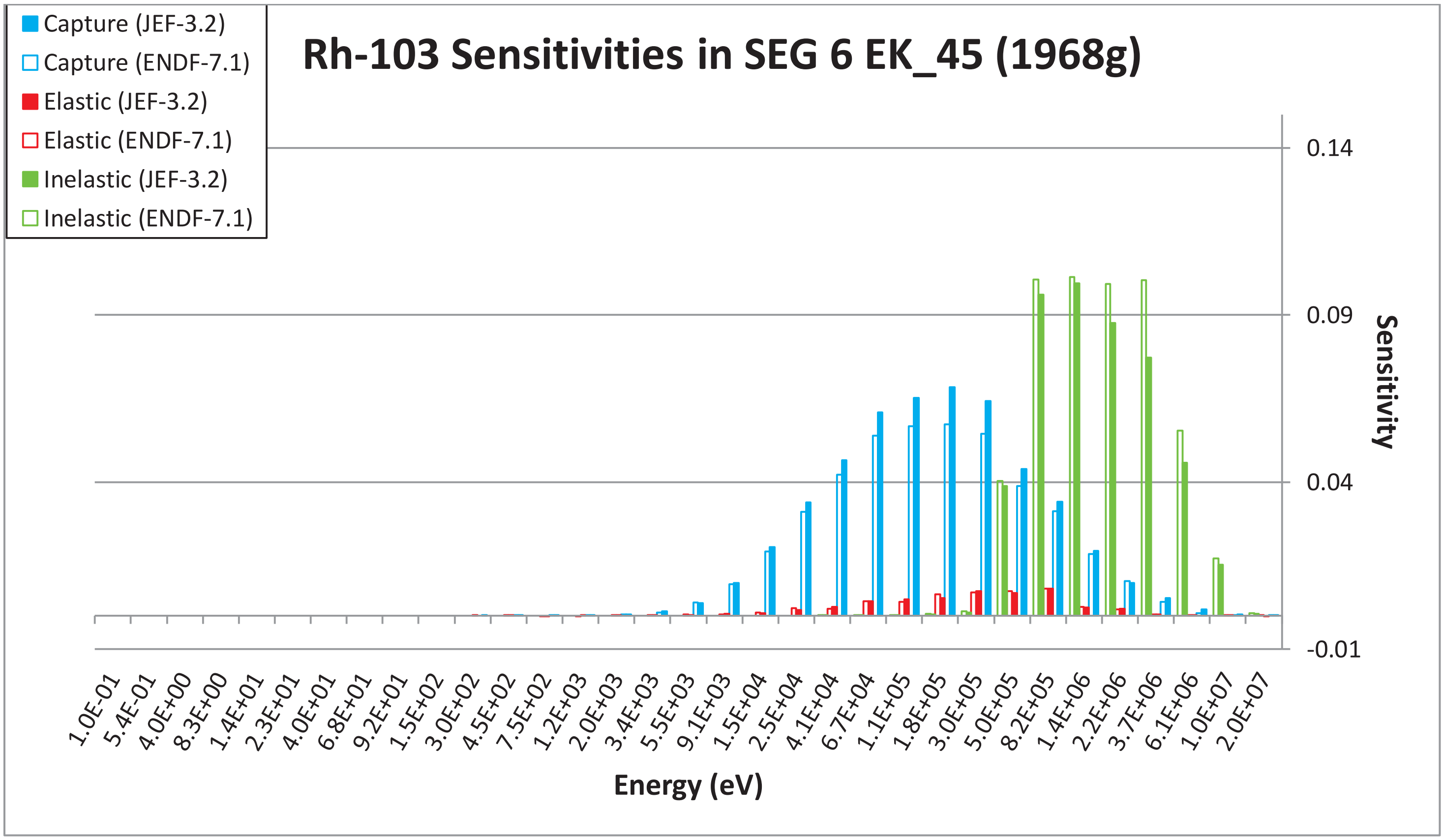


Figure 4.31 Rh-103 sensitivities in SEG 6 EK_45.

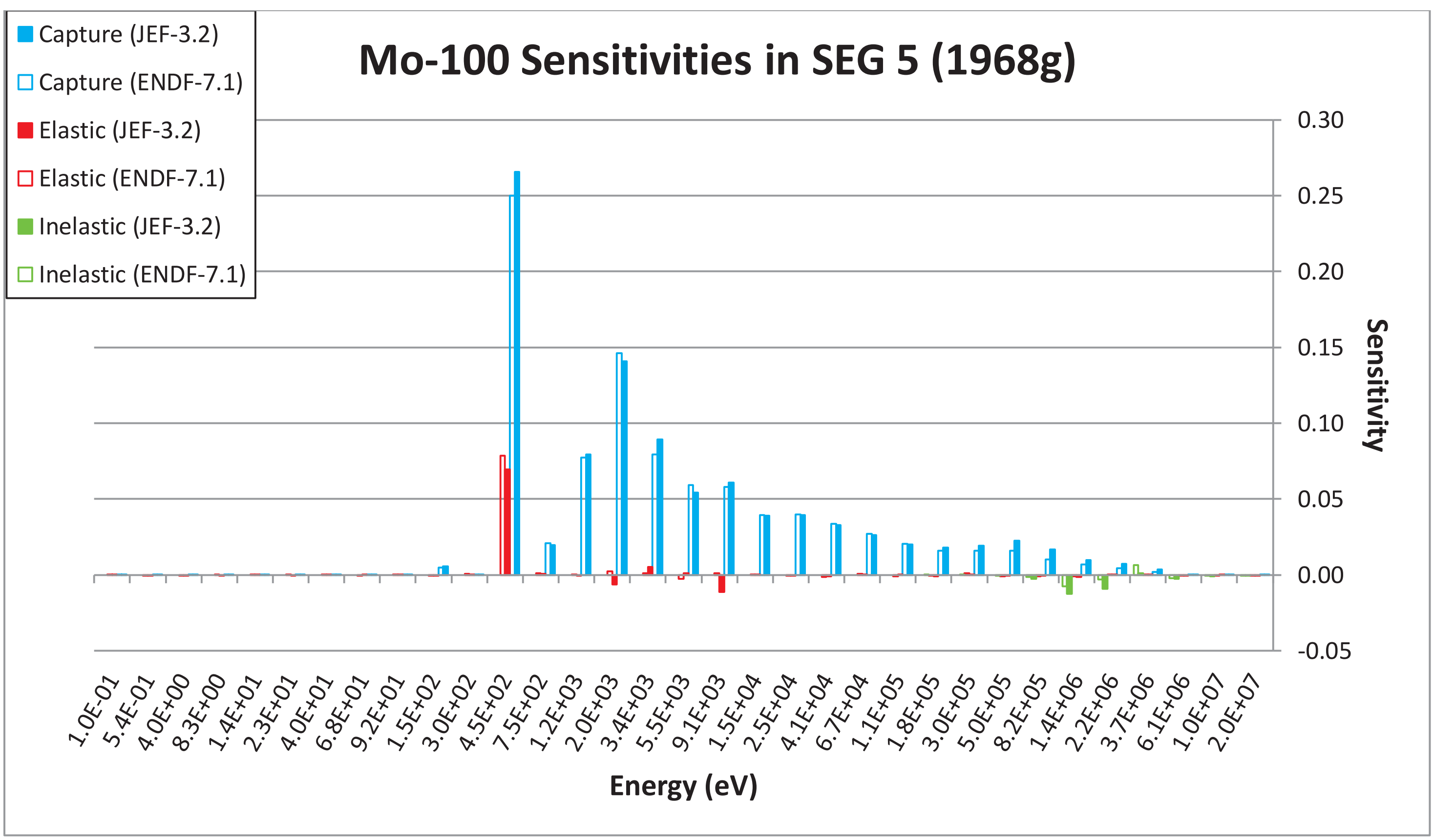


Figure 4.32 Mo-100 sensitivities in SEG 5.

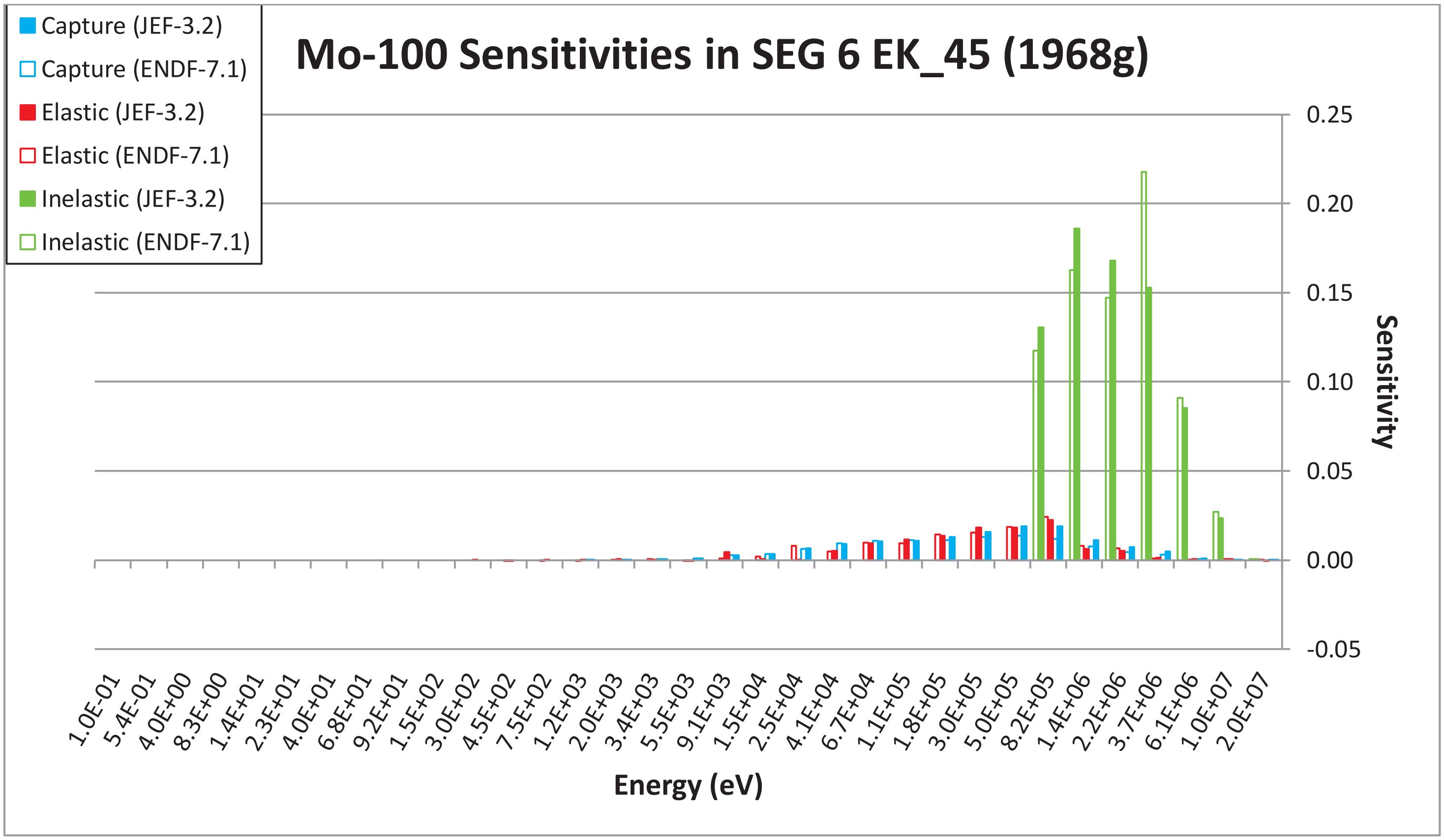


Figure 4.33 Mo-100 sensitivities in SEG 6 EK_45.

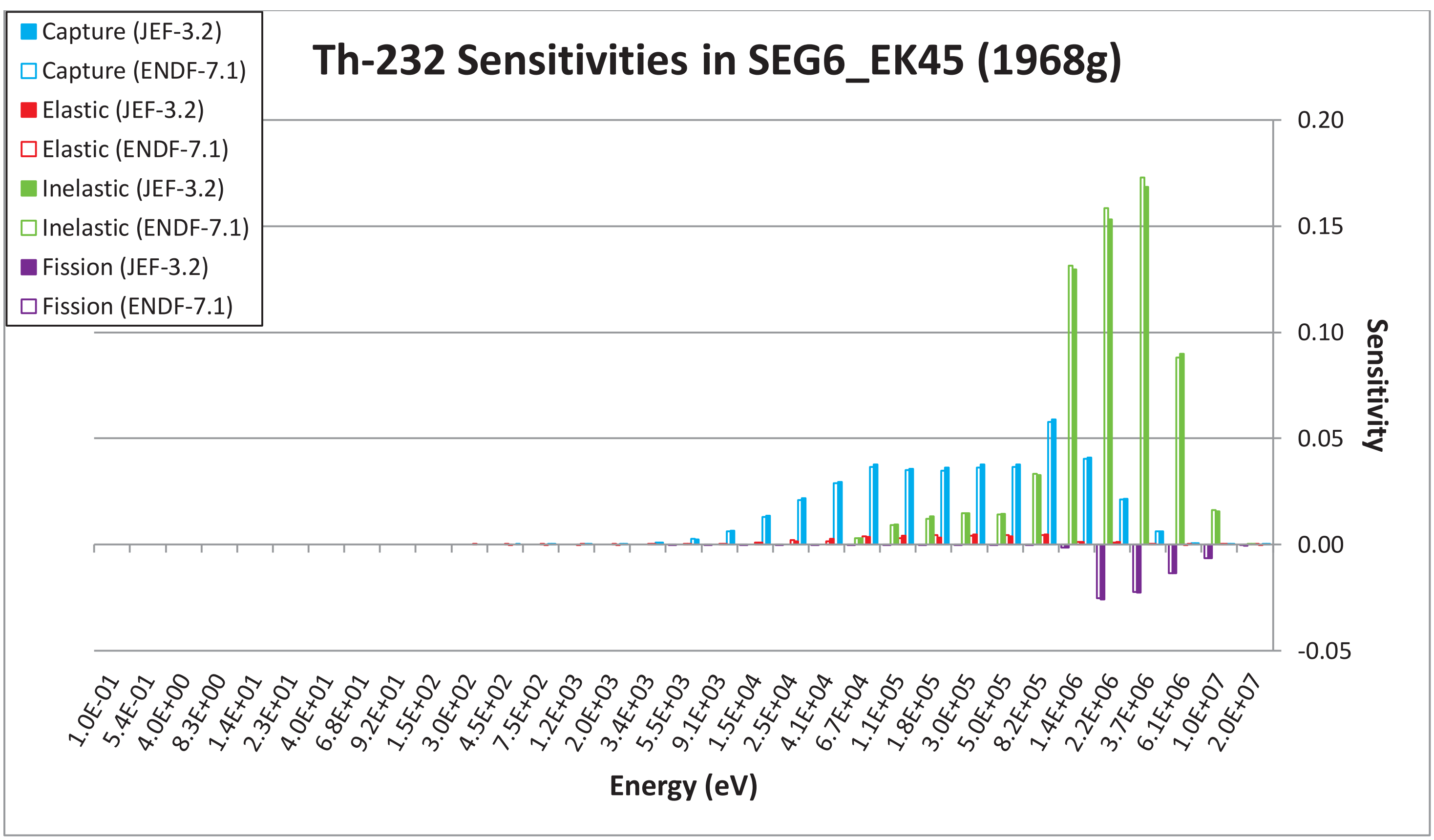


Figure 4.34 Th-232 sensitivities in SEG 6 EK_45.

# 5. CONCLUSIONS

In this report we have illustrated the preliminary analysis of several experimental campaigns, named SEG, performed at the Rossendorf facility in East Germany. The interest of the analyzed reactivity oscillation measurements resides in the characteristic of the adjoint energy shape obtained at the facility using appropriate filters. These experimental configurations have permitted to obtain measurements that enhance either the absorption or scattering components. In this way, the experiments belong to the class of the so called "elemental" experiments that allow to separate effects and, therefore, gain information on specific quantities, corresponding in this case to isotope reactions.

An extraordinary challenge in the calculational analysis was represented by the extremely low values of the measured reactivities for which the modern calculational tools, Monte Carlo methods, are ill suited. However, the access to a recently developed capability in the French TRIPOLI code has allowed one to overcome this problem.

A full set of C/E using different libraries has been obtained and further analysis is needed in order to assess the reliability of the results. To this latter purpose, the sensitivity analysis, of which preliminary results have been presented, will be of undoubtable usefulness. However, further sensitivity capabilities are still needed, in particular related to the indirect effects. It is planned that in the future the use of a newly developed version of another Monte Carlo code, SERPENT, will allow one to obtain these needed quantities. Finally, it has to be stressed that the final aim of using the SEG experiments is to introduce the observed C/E's, the associated calculational and experimental uncertainties, and the related sensitivities in a comprehensive data assimilation procedure in order to obtain improved neutron cross sections that will provide feedback to the evaluators of the current most used nuclear data libraries.

## REFERENCES


[1] T. Kampf, P. Liewers, “Der Rossendorfer Ringzonenreaktor (RRR) – ein Instrument fur reaktorphysikalische Untersuchungen”, *Kernenergie*, **volume (6),** pp. 300 – 305 (1963).

[2] U. Helwig, W. Boessert, “Decommisioning of the Nuclear Facilities of VKTA at the Rossendorf Research Site”, Proc. Int. Conf. *Waste Management Conference*, Tuscon, AZ, February 23 – 27 (2003).

[3] K. Fahrmann, D. Albert, H. U. Barz, K. Dietze, W. Hansen, D. Hedderich, G. Huttel, H. Krause, E. Lehmann, B. Osmera, W. Vogel, “Der Einsatz des Rossendorfer Rinzonenreaktors fur Untersuchungen zur Physik Schneller Reaktoren”, *Kernenergie*, **volume (25/2)**, pp. 464- 471.

[4] K. Dietze, “The Rossendorf RRR/SEG – Facility”, LEPH-93-230, CEA Cadarache. (1993).

[5] K. Dietze, K. Faehrmann, G. Huettel, E. Lehmann, “Neutron data check for structural materials by reactivity measurements in a fast facility with energy-independent adjoint flux,” Kernenergie 29/11, p. 401-409, (1986).

[6] K. Dietze, K. Faehrmann, G. Huettel, W. Hansen, H. Kumpf, E. Lehmann, “Neutron Absorption Data Analysis by Means of Integral Experiments in Fast Critical Facilities,” Kerntechnik 53/2, p. 143-149, (1988).

[7] K. Dietze, “Integral Test of JENDL – 3.2 Data by Analysis of Sample Reactivity Measurements in Fast Critical Facilities,” Presented February 17, (2000).

[8] K. Dietze K., “Integral Test of JENDL – 3.2 Data by Re-analysis of Sample Reactivity Measurements at SEG and STEK Facilities,” Proceedings of the 2000 Symposium on Nuclear Data, November 16-17, Tokai, Japan, (2000).

[9] E. Lehmann, W. Hansen, G. Huettel, H. Kumpf, D. Richter, “ Investigations in a Fast Reactor Assembly with a Strongly Energy-Independent Adjoint Function,” ZfK – 729, December (1990).

[10] S. M. Lumbanraja, “Analysis of Sample Reactivity Measurements in the Rossendorf SEG-7 Configuration,” Institut National Polytechnique de Grenoble, (1994).

[11] K. Faehrmann, E. Lehmann, “A Fast-Thermal Coupled System with Energy-Independent Adjoint Flux,” Kernenergie 24, p. 431-433, (1981).

[12] E. Lehmann, K. Faehrmann, G. Huettel, H. Krause, H. Kumpf, “The Method of Energy-Independent Adjoint Flux and its Perfection by the SEG-5 Configuration,” Kernenergie 29/1 p. 30-34, (1986).

[13] E. Lehmann, G. Huettel, H. Krause, H. Kumpf, “A Fast Critical Reactor Assembly with Strong Energy Dependence of Adjoint Flux,” Kernenergie 34/1 p. 9-12, (1991).

[14] K. Dietze, “Analysis of the Rossendorf SEG Experiments Using the JNC Route for Reactor Calculations,” O-arai Engineering Center, Japan Nuclear Cycle Development Institute, November, (1999).

[15] K. Dietze, “Integral Test of JENDL-3.2 Data by Re-analysis of Sample Reactivity Measurements at Fast Critical Facilities,” O-arai Engineering Center, Japan Nuclear Cycle Development Institute, February, (2001).

[16] K. Dietze, G. Rimpault, “An Analysis of Sample Reactivity Measurements in Rossendorf SEG Configurations Using the JEF-2 Data Base,” JEF/DOC-451, CEA – CEN Cadarache / DRN DER SPRC, 13108 St. Paul Lez Durance CEDEX, France.

[17] K. Dietze, G. Rimpault, “Integral Test of JEF2 Self-Shielding Data Using the JEF2/ERANOS Scheme,” LEPH-94-220.

[18] K. Dietze, G. Rimpault, “Reanalysis of the SEG6 Experiments Using the JEF2/ECCO/ERANOS Scheme,” LEPH-94-206.

[19] K. Dietze, G. Rimpault, “Analysis of Sample Reactivity Measurements in the RRR/SEG-5 Configuration with the JEF-2 Nuclear Data Base,” LEH-93-237.

[20] K. Dietze, H. Kumpf, “Eine Analyse der Kerndaten von Spaltprodukten durch Reaktivitaetsmesungen in Schnellen Reaktorkonfigurationen mit energieunabhangiger Einflussfunktion,” Kernenergie 34/1, p. 1-9, (1991).

[21] E. Lehmann, D. Albert, K. Dietze, K. Faehrmann, W. Hansen, G. Huettel, H. Wand, B. Osmera, “Ergebnisse der Untersuchung einer schnellen Reaktokonfiguraion mit stark heterogener Zellstruktur,” Akademie Der Wissenschaften Der DDR, November (1984).

[22] Monte Carlo N-Particle Transport Code System Including MCNP6.1, MCNP5-1.60, MCNPX-2.7.0 and Data Libraries. Initial MCNP6 Release Overview – MCNP6 version 1.0. Los Alamos National Laboratory, Los Alamos, New Mexico, August (2013).
[23] A. Hummel, "Re-analysis of the RRR/SEG Fast Thermal Coupled Facility," *PHYSOR 2016 Conference*, Sun Valley, ID (2016).
[24] Tripoli-4 Version 8, User Guide, Rapport CEA, CEA Saclay, Direction des systemes d'information, http://www.oecd-nea.org/tools/abstract/detail/nea-1716/ , (2012).
[25] M. Salvatores, "Integral Experiments for Reactor Physics Validation," Presentation at Summer 2015 MEV School, Argonne National Laboratory (2015).
[26] D. Albert, K. Fahrmann, E. Lehmann, E. Seifert, "Investigation of a moderated Sb-Be photoneutron source and its application to the determination of the neutron importance function," Nuclear Instruments and Methods in Physics Research, Vol. 185, Issues 1-3, p. 387-392, June (1981).
[27] D. Albert, U. Bruckner, W. Hansen, W. Vogel, "Determination of Light Efficiency of Stilbene Scintillators and their Application to In-Core Spectrometry of Fast Neutrons, Nuclear Instruments and Methods, Vol. 200, p. 397-402, January (1982).
[28] Foell W. K. "Small-Sample Reactivity Measurements in Nuclear Reactors," Prepared under the direction of the American Nuclear Society for United Sates Atomic Energy Commission, American Nuclear Society, 244 E. Ogden Avenue, Hinsdale, Illinois 60521, (1972).
[29] Weinberg A. M., Schweinler H. C., "The Theory of Oscillating Absorbers in a Chain Reactor," Physics Review, 74, 851, (1948).
[30] E. Lehmann, W. Hansen, G. Huttel, H. Kumpf, D. Richter, "Investigations in a Fast Reactor Assembly with a Strongly Energy-Dependent Adjoint Function", Zfk-729, December (1990).
[31] J. J. Duderstadt, L. J. Hamilton, *Nuclear Reactor Analysis*, John Wiley & Sons, Inc., (1976).
[32] H. Rief, "Generalized Monte Carlo perturbation algorithms for correlated sampling and a second-order Taylor series approach," *Annals of Nuclear Energy*, Vol. 11, p. 455 – 476 (1984).
[33] J. Hoogenboom, *Adjoint Monte Carlo methods in Neutron Transport Calculations,* Delft University Press (1977).
[34] B. Kiedrowski, S. Swindell, *Adjoint Weighting for Continuous Energy Monte Carlo Radiation Transport,* University of Wisconsin, Ph.D. Thesis (2009).
[35] M. Aufiero, A. Bidaus, M. Hursin, J. Leppanen, G. Palmiotti, S. Pelloni, P. Rubiolo, "A Collision history-based approach to Sensitivity/Perturbatin calculations in the continuous energy Monte Carlo code SERPENT," *Annals of Nuclear Energy*, Vol. 85, p. 245 – 258, November (2015).
[36] G. Truchet, P. Leconte, Y. Peneliau, A. Santamarina, F. Malvagi, "Continuous-Energy Adjoint Flux and Perturbation Calculation using the Iterated Fission Probability Method in Monte Carlo Code TRIPOLI-4 and Underlying Applications," Joint International Conference on Supercomputing in Nuclear Applications and Monte Carlo, Paris, France, October 27-31 (2013).
[37] Y. Nauchi, T. Kameyama, "Development of Calculation Technique for Iterated Fission Probability and Reactor Kinetic Parameters Using Continuous Energy Monte Carlo Methods," *Journal of Nuclear Science and Technology*, Vol. 47, p. 977 – 990, (2010).
[38] A. M. Weinberg, "Current Status of Nuclear Reactor Theory," *American Journal of Physics*, Vol. 20, p. 401 412 (1952).
[39] G. Truchet, P. Leconte, A. Santamarina, "Implementation and Validation of Reference Sensitivity Profile Calculations in TRIPOLI4," PAPER TO BE RELEASED.
[40] G. Truchet, P. Leconte, P. Archier, J. Tommasi, A. Santamarina, "Sodium Void Reactivity Effect Analysis Using the Newly Developed Exact Perturbation Theory in Monte Carlo Code TRIPOLI-4," PHYSOR 2014 – The Role of Reactor Physics toward a Sustainable Future, Kyoto, Japan, September 28 – October 3 (2014).
[41] G. Truchet, P. Leconte, A. Santamarina, E. Brun, F. Damian, A. Zoia, "Computing adjoint-weighted kinetics parameters in TRIPOLI-4 by the Iterated Fission Probability method," Annals of Nuclear Energy, Vol. 85, p. 17 – 26, (2015).

[42] P. Liewers, “Reaktorphysikalische Forschungen in der DDR” Sitzungsberichte der Leibniz-Sozietat, 89, p. 39 – 54 (2007).

# APPENDIX A

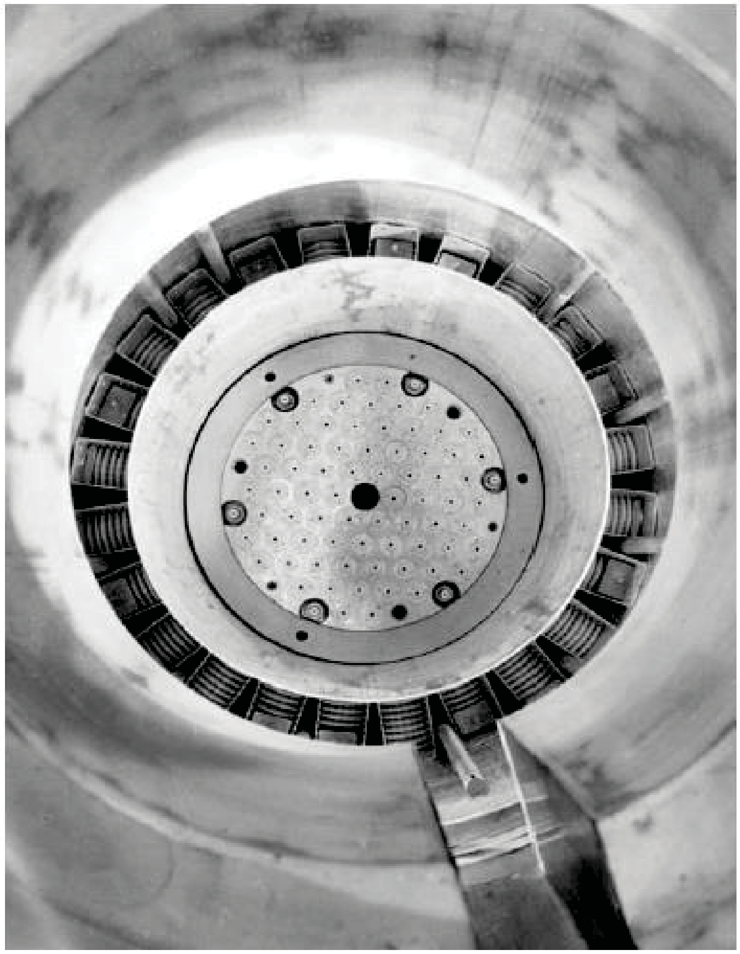

Figure A.1. Picture from top of the core of the SEG lattice inserted into the RRR [42].